Thymic self-recognition-mediated TCR signal strength modulates antigen-specific CD8$^+$ T cell pathogenicity in non-obese diabetic mice

Chia-Lo Ho[1], Li-Tzu Yeh[2], Yu-Wen Liu[3], Jia-Ling Dong[4], Huey-Kang Sytwu[1,2,3,4]

[1]Molecular and Cell Biology, Taiwan International Graduate Program, Academia Sinica and Graduate Institute of Life Sciences, National Defense Medical Center, Taipei, Taiwan.

[2]Department and Graduate Institute of Microbiology and Immunology, National Defense Medical Center, Taipei, Taiwan.

[3]National Institute of Infectious Disease and Vaccinology, National Health Research Institutes, Miaoli, Taiwan.

[4]Graduate Institute of Life Sciences, National Defense Medical Center, Taipei, Taiwan.

Address correspondence and reprint request to Dr. Huey-Kang Sytwu, National Institute of Infectious Diseases and Vaccinology, National Health Research Institutes, 35, Keyan Road, Zhunan Town, Miaoli County 350, Taiwan

TEL: +886-37-206166, ext 31011;

FAX: 886-2-87921774

E-mail address of corresponding author: sytwu@nhri.org.tw

Competing interests: All the authors declare no competing interests.

Key words: autoimmune diabetes, CD8, CD5

Abstract

Our understanding of autoimmune diabetes underscores the critical involvement of $CD8^+$ T cells recognizing islet-specific antigens. However, the influence of thymic positive selection on diabetogenic $CD8^+$ T cell development remains unclear. Using CD5 marker representing T-cell receptor (TCR) signal strength, we illustrated that naïve $CD5^{hi}CD8^+$ T cells of non-obese diabetic (NOD) mice with enhanced TCR signals displayed predisposed differentiated/memory T cell traits with increased activation and proliferation upon TCR stimulation, compared to $CD5^{lo}$ counterparts. Additionally, $CD5^{hi}CD8^+$ T cells exhibited gene expression landscape similar to effector T cells and exacerbated disease in transfer model. Interestingly, the protective effects of transgenic phosphatase Pep expression, which lowers TCR signaling and diabetes incidence, were abolished in NOD strain 8.3 with high CD5 expression linked to increased thymic positive selection. Strikingly, TCR repertoire analysis identified higher frequencies of autoimmune disease-related clonotypes in naïve $CD5^{hi}CD8^+$ cells, supporting that distinct effector functions arise from intrinsic TCR repertoire differences. Overall, $CD5^{hi}CD8^+$ clones may be potential targets for autoimmune diabetes treatment.

Introduction

T cells play a crucial role in inducing immunity by recognizing peptides presented on MHC molecules through their TCR during pathogen infection. The strength of the TCR's reactivity to the foreign antigen is contributed by both the affinity of the TCR for that antigen and the basal TCR signaling level of the T cell, which is determined by weak interactions between the TCR and self-peptides presented during T cell development (1, 2). Previous studies have shown that T cell self-reactivity with weak interaction between TCR and self-peptide-MHC (self-pMHC) not only instructs T cell development and activation thresholds, but also influences their functional response (2-4). It is noteworthy that the strength of the weak interaction can be evaluated through CD5, whose expression level is considered proportional to T cell self-reactivity in the developmental stage, and may reflect the responses of T cells to foreign-pMHC complexes in the future (2, 5, 6).

CD5 is a scavenger receptor cysteine-rich protein expressed on T and B cells that regulates TCR and B-cell receptor signaling (7, 8). It functions as a scaffold protein for the recruitment of phosphatase SHP-1 and E3-ubiquitin ligases CBL and CBLB, to reduce the phosphorylation of proximal TCR signaling molecule Zap70, thereby inhibiting TCR-mediated signaling (9). CD5, as a negative regulator for TCR signaling, also plays a crucial role in fine-tuning the process of positive and negative selection during thymocyte development (8, 10). Specifically, thymocytes with higher self-reactivity TCRs induce CD5 expression, which helps them adapt to strong TCR signaling and reduces the likelihood of negative selection. This, in turn, promotes thymocyte positive selection and broadens the affinity spectrum of the TCR repertoire during the TCR self-recognition process. Therefore, the expression of CD5 is not only a surrogate marker for the strength of TCR-self-peptide-MHC interactions during development but also reflects the intrinsic response set point of T cells to a signal (5, 10). This selection process enriches the mature $CD4^+$ T

24 cell repertoire with clones that exhibit increased responses to self-peptide-MHC, thereby
25 displaying enhanced peripheral immune responses to pathogens and autoantigens *in vivo* (5, 11,
26 12). Not only in $CD4^+$ T cells, previous study has also shown that $CD5^{hi}$ population in $CD8^+$ T
27 cells, characterized by higher reactivity to self-peptide-MHC, are prone to positive selection (5,
28 13). In diabetes-prone NOD mice, though negative selection in central tolerance limits the early
29 contribution of high-avidity T cells to disease development, prolonged inflammation in pancreatic
30 islets still drives the avidity maturation of islet-specific glucose-6-phosphatase catalytic subunit-
31 related protein (IGRP)-specific $CD8^+$ T cells, leading to increased cytotoxicity towards β cells (14-
32 16). This suggests that mechanisms other than incomplete thymic negative selection are involved
33 in generating autoreactive T cells. Here, we investigate whether the CD5-correlated self-pMHC
34 reactivity, which attributes to TCR signal strength in autoreactive $CD8^+$ T cells during thymic
35 positive selection, contributes to the development of autoimmune disease.

36 The NOD mouse model is commonly used for studying autoimmune diabetes. NOD mice
37 spontaneously develop autoimmune diabetes similar to human type 1 diabetes (T1D) with
38 immune-mediated destruction of β cells in the pancreas (17-20). Additionally, genetic variation
39 influences cell lineage decisions during T cell development, affecting positive and negative
40 selection processes and contributing to the emergence of pathogenic $CD4^+$ T cells in diabetes-
41 prone NOD mice (16). Both $CD4^+$ and $CD8^+$ T cells play critical roles in pathogenic diabetogenesis,
42 in which $CD4^+$ T cells drive disease onset and $CD8^+$ T cells mediate β cell destruction (21).
43 However, little is known about the factors affecting $CD8^+$ T cell activity, and the extent to which
44 $CD8^+$ T cell reactivity to self-pMHC during thymic positive selection affects its responses to
45 autoantigens during autoimmune processes remains unclear.

46 We hypothesize that the spectrum of $CD8^+$ T cell diabetogenicity correlates with its

47 expression level of CD5, representing the gratitude of self-pMHC-mediated TCR signaling. In this
48 study, we use *Ptpn22* (22-24) and islet antigen-specific 8.3 TCR transgenic (NOD8.3) (25, 26)
49 mice in addition to conventional NOD mice to investigate this hypothesis. The *Ptpn22* gene
50 encodes PEST domain-enriched tyrosine phosphatase (Pep), which negatively regulates TCR
51 signaling. We have previously demonstrated that different modulation of Pep in effector and
52 regulatory $CD4^+$ T cells leads to attenuation of autoimmune diabetes in distal Lck promoter-driven
53 Pep transgenic NOD mice (dLPC/NOD) (27). Here, we crossed dLPC/NOD to NOD8.3 transgenic
54 mice to generate dLPC/NOD8.3 double transgenic mice and further investigate whether transgenic
55 Pep-mediated protective potential in $CD4^+$ T cells with lower TCR signaling (27) can also be
56 applied to an autoantigen-specific $CD8^+$ T cells with higher CD5 and TCR basal signaling in 8.3
57 TCR transgenic mice. Our data reveal that the activation and proliferation of $CD8^+$ T cells from
58 dLPC/NOD8.3 mice was not attenuated, compared to $CD8^+$ T cells from NOD8.3 mice, suggesting
59 that a dominant role of autoantigen reactivity in $CD8^+$ T cell with high TCR basal signaling and
60 CD5 overrides the transgenic Pep-mediated signaling attenuation during autoimmune
61 diabetogenesis. Exploring a potential modulation of CD5-dependent TCR basal signaling and its
62 impact on T cell reactivity may offer a promising therapeutic strategy for the treatment of T1D in
63 the future.
64
65
66
67
68
69

70 **Results**

71 **Phenotypic difference exists in naïve CD5^{hi}CD8^{+} and CD5^{lo}CD8^{+} T cells of NOD**

72 **mice.**

73 Given that CD5 can serve as a surrogate marker of TCR basal signal strength, which
74 correlates with T cell's self-recognition capability, our initial analysis aimed to determine whether
75 naïve (CD44^{lo}CD62L^{hi}) CD8^{+} T cells from NOD mice with different CD5 levels (CD5^{hi}CD8^{+} and
76 CD5^{lo}CD8^{+} T cells) display distinct levels of the TCR basal signal markers p-CD3ζ and p-Erk.
77 The histograms and gMFI analysis revealed significantly increased levels of p-CD3ζ and p-Erk in
78 CD5^{hi}CD8^{+} T cells, in comparison to CD5^{lo}CD8^{+}, while the amounts of p-CD3ζ and p-Erk in total
79 naive CD8^{+} T cells were generally lied between the CD5^{hi} and CD5^{lo} subsets (Figure 1, A and B,
80 and Supplementary Figure 1A) in both spleen and pancreatic lymph nodes (PLNs). This result
81 implies an enhanced signaling potential and activation status of CD5^{hi}CD8^{+} T cells, compared to
82 CD5^{lo}CD8^{+} cells, in NOD mice. Since two critical T-box transcription factors, T-bet and Eomes,
83 are regulators of differentiation and effector functions of CD8^{+} T cells (28-30), we further
84 investigated whether intrinsic differences in self-recognition capabilities and subsequent
85 functional heterogeneity between CD5^{hi}CD8^{+} and CD5^{lo}CD8^{+} populations correlate the expression
86 levels of T-bet and Eomes. Our results indicated higher levels of T-bet and Eomes in the naïve
87 CD5^{hi}CD8^{+} population in both spleen and PLNs, compared to CD5^{lo} counterparts (Figure 1C and
88 Supplementary Figure 1B). Elevated expressions of T-bet and Eomes in CD8^{+} T cells have been
89 reported to play critical role in promoting T cell migration to inflamed tissues through induction
90 of chemokine receptors (31, 32) in addition to their association with the differentiation of activated
91 CD8^{+} T cells (28). These upregulated T-bet and Eomes in naïve CD5^{hi}CD8^{+} T cells (Figure 1C)
92 were consistent with elevated levels of Granzyme B, TNF-α, IFN-γ and IL-2 (Figure 1D and

93 Supplementary Figure 1C), indicating the potential of these cells in cytokine production and
94 effector functions. Additionally, $CD5^{hi}CD8^{+}$ subset expressed higher level of chemokine receptor
95 CXCR3 (Figure 1E) than $CD5^{lo}CD8^{+}$ counterparts, a characteristic often associated with effector
96 and memory T cell populations, implying a enhanced ability for migration and localization in
97 response to specific chemotactic signals.

98 Building upon our observations of the phenotypic and functional differences between naïve
99 $CD5^{hi}$ and $CD5^{lo}CD8^{+}$ T cell subsets in NOD mice (Figure 1, A-D), as well as previous research
100 highlighting T-bet- and Eomes-related regulatory mechanisms within $CD8^{+}$ T cell populations (3,
101 28), we next sought to investigate whether CD5-associated self-recognition capabilities influence
102 specific gene regulation in $CD8^{+}$ T cells via distinct levels of T-bet and Eomes. It is well
103 documented that T-bet and Eomes work together to control CD122 expression, a common β chain
104 receptor for IL-2 and IL-15, which is crucial for the survival of IL-15-dependent memory $CD8^{+}$ T
105 cells (30, 33). Additionally, CD122, in cooperation with CD127 (IL-7Rα), represents essential
106 receptors for IL-2, IL-15, and IL-7. They play a pivotal role in regulating $CD8^{+}$ T cell subsets
107 during the memory phase of the immune response (34-37), which is crucial for maintaining
108 memory T cell homeostasis. As shown in Figure 1E, higher expression of CD122 and CD127 was
109 observed in the $CD5^{hi}CD8^{+}$ population, supporting that the overall phenotypic traits of naïve
110 $CD5^{hi}CD8^{+}$ T cells resemble those of memory $CD8^{+}$ T cells (Figure 1E), particularly in their ability
111 to maintain T cell homeostasis.

112 In addition to distinct expression patterns of these memory T cell-related homeostasis
113 markers, like CD122 and CD127 (Figure 1E), we also identified higher expressions of other T cell
114 activation markers, including CD69 (38, 39), PD-1 (40, 41), and KLRG-1 (37, 42), in naïve
115 $CD5^{hi}CD8^{+}$ T cells compared to their $CD5^{lo}$ counterparts (Figure 1F). Similar to PD-1, the

116 activation marker CD44, an adhesion molecule and marker for antigen-experienced T cells, was
117 up-regulated in the $CD5^{hi}CD8^{+}$ population (Figure 1F), as previously reported (3, 34, 43, 44).
118 Additionally, $CD5^{hi}$ cells also exhibit elevated expression of CD25 (IL-2Rα), supporting the
119 presence of intrinsic phenotypic distinction between the $CD5^{hi}$ and $CD5^{lo}$ populations in NOD
120 naïve $CD8^{+}$ T cells (Figure 1F). Since the increased number of islet antigen IGRP-specific $CD8^{+}$
121 T cells positively correlate with insulitis progression both in human T1D and NOD mice, we thus
122 used MHC-tetramer technique to trace $IGRP_{206–214}$-specific $CD8^{+}$ T cells in NOD mice. Our results
123 revealed that $CD5^{hi}CD8^{+}$ T cells compared to $CD5^{lo}CD8^{+}$ counterpart had significant increase in
124 IGPR-tetramer staining level (Figure 1G), suggesting that $CD5^{hi}CD8^{+}$ T cells with higher self-
125 antigen recognizing ability contribute more to islet-destructive pathogenesis in T1D. Collectively,
126 in line with previous findings, our results indicate that the phenotypic characteristics of naïve
127 $CD5^{hi}CD8^{+}$ T cells resemble those of effector/memory T cells and confer distinct functional
128 capabilities in autoimmune diabetogenesis compared to $CD5^{lo}CD8^{+}$ cells.
129

130 **Differential gene expression profiling of naïve $CD8^{+}$ T cells stratified by CD5**
131 **levels identifies autoimmune disease-associated gene signatures.**

132 To unveil the underlying differences in phenotypic characteristics between $CD5^{hi}CD8^{+}$ and
133 $CD5^{lo}CD8^{+}$ T cells, we analyzed the gene expression profiling by sorting the 10% upper and lower
134 CD5-expressing naïve $CD8^{+}$ T cells from prediabetic mice at the age of 6 to 8 weeks old (Figure
135 2A). We performed differentially expressed genes (DEGs) analysis using multiple platforms and
136 bioinformatic tools to compare the transcriptomic profiles of $CD5^{hi}$ versus $CD5^{lo}$ T cells. Our
137 DEGs results showed that a total of 185 genes were found to be differentially expressed between
138 $CD5^{hi}$ and $CD5^{lo}$, with a fold change greater than 2 and a p-value less than 0.05 cutoffs; within

139 these genes, 133 were upregulated and 52 were downregulated (Supplementary Table 1 and 2).
140 The significantly upregulated DEGs revealed by the volcano plot (Figure 2B) in $CD5^{hi}$ subset
141 include memory T cell homeostasis marker *Il2rb* (CD122), T cell effector/memory function-
142 associated markers *Tbx21*, *Eomes*, and chemokine receptor *Cxcr3*, consistent with the results
143 obtained in Figure 1. Interestingly, the *Xcl1* gene, which encodes the ligand XCL1 exclusively
144 binding to XCR1 on dendritic cells and facilitating antigen-specific $CD8^+$ T cell expansion, IFN-
145 γ secretion and cytotoxicity, was also upregulated in the $CD5^{hi}$ population (28, 45, 46), implying
146 that $CD5^{hi}CD8^+$ T cells are poised for efficient priming upon antigen encounter.

147 To further characterize DEGs for their functional implications, we performed gene set
148 analysis based on the gene ontology (GO). A gene-concept network by $CD5^{hi}$ versus $CD5^{lo}$ DEGs
149 was associated with the three GO terms: external side of plasma membrane (GO:0009897), T cell
150 activation (GO:0042110), and cytokine production involved in immune response (GO:0002367)
151 (Supplementary Figure 2A). Among the notable findings, genes such as *Cd5*, *Cd83*, *Eomes*, *Xcl1*,
152 *Tbx21*, *Il18rap*, *Klra1*, *Cxcr3*, and *Pdcd1* were significantly upregulated within $CD5^{hi}CD8^+$ T cells,
153 with fold changes equal to or greater than 2. Specifically, within the GO term cytokine production
154 involved in immune response, genes such as *Crlf2*, *Kit*, *F2rl1*, *Xcl1*, *Tbx21*, *Tnfrsf1b* and *Il18rap*
155 showed upregulated expression patterns. Overall, these results provide insights into the potential
156 mechanisms underlying T cell activation and cytokine production in $CD5^{hi}$ population.

157 To thoroughly analyze the intrinsic kinetics and expression profiles of $CD5^{hi}CD8^+$ versus
158 $CD5^{lo}CD8^+$ T cells under conditions resembling antigen encounter, we cross-referenced our
159 findings with a dataset that delineates the functional relevance of ten gene clusters established in
160 a prior study (47). This study identified core transcriptional signatures governing $CD8^+$ T cell
161 activation and effector/memory cell differentiation during infections, defining ten temporal gene-

162 regulated patterns (clusters I~X) in $CD8^+$ T cells. Using a $\chi 2$ test to examine gene expression
163 variations in these ten clusters between $CD5^{hi}$ and $CD5^{lo}$ cells (Table 1), we found that the $CD5^{hi}$
164 subset has a significantly higher expression of genes linked to the initial cytokine or effector
165 response (cluster I) and preparation for cell division (cluster II). Additionally, it exhibits a
166 moderately higher expression of genes associated with cell cycle and division (cluster III), early
167 effector and late memory (cluster V), short-term effector or memory (clusters IX), and late effector
168 or memory (clusters X) in the $CD8^+$ T cell response (Table 1 and Supplementary Figure 2B).
169 Collectively, these data support that the $CD5^{hi}$ T cells are better prepared for initial activation and
170 late memory formation compared to the $CD5^{lo}$ population.

171 In addition, we performed gene set enrichment analysis (GSEA) on DEGs using the Broad
172 Institute's GSEA desktop software. GSEA analysis indicate that $CD5^{hi}$ cells were enriched for GO
173 terms such as T cell activation (GO:0042110), external side of the plasma membrane
174 (GO:0009897), positive regulation of immune system process (GO:0002684), regulation of
175 catalytic activity (GO:0050790) and other GO terms with similar biological process (BP) functions
176 (Figure 2C, Supplementary Figure 2C and Supplementary Table 3), similar to the results in
177 Supplementary Figure 2A. Collectively, these results of cluster analysis (Table 1) and GSEA
178 (Figure 2C) indicate that $CD5^{hi}CD8^+$ T cells in NOD mice possess a greater inherent potential for
179 T cell activation and memory cell formation, which may contribute to the initiation and persistence
180 of autoimmune diabetes.

181 Moreover, we analyzed DEGs by applying Kyoto Encyclopedia of Genes and Genomes
182 (KEGG) database to further investigate whether $CD5^{hi}CD8^+$ subset is enriched in any potential
183 disease-related pathways. Strikingly, two pathways stood out: the inflammatory bowel disease
184 (IBD)- and type 1 diabetes mellitus-associated pathways (Figure 2D). The enrichment results for

185 IBD and TID pathways suggest that naïve $CD5^{hi}CD8^{+}$ T cells with heightened self-reactivity have
186 the intrinsic capacity to induce T1D and IBD. In summary, our data from gene-concept interactions,
187 GSEA and KEGG pathways reveal distinct phenotypes in $CD5^{hi}CD8^{+}$ subset, indicating their
188 potential for autoimmune predisposition even in their naïve state.
189

190 $CD5^{hi}CD8^{+}$ and $CD5^{lo}CD8^{+}$ T cell subsets have distinct activation and 191 proliferation levels.

192 To examine whether variations in self-recognition, as indicated by CD5 expression,
193 determine diabetogenic $CD8^{+}$ T cell proliferation after TCR stimulation, we isolated naïve $CD8^{+}$
194 T cells and subjected them to 2 days of dose-dependent TCR stimulation using various
195 concentrations of anti-CD3 in combination with a consistent concentration of anti-CD28 (Figure
196 3A). Subsequently, we characterized phenotypic and functional distinctions within the 5% upper
197 and lower CD5-expressing subsets of $CD8^{+}$ T cells. Unlike the lower 5% $CD8^{+}$ groups showing
198 moderate change, the upper 5% $CD8^{+}$ groups exhibited much more significant increase in CD5
199 levels in TCR stimulation dose-dependent manner (Figure 3B). The $CD5^{hi}CD8^{+}$ subset also
200 showed higher p-CD3ζ abundance compared to $CD5^{lo}CD8^{+}$ subset across all TCR stimulation
201 doses. Specifically, p-CD3ζ in $CD5^{hi}CD8^{+}$ peaked at 1.25 μg/ml anti-CD3 stimulation, then
202 gradually declining with increased TCR stimulation doses, possibly due to its faster kinetic
203 expression compared to other T cell activation signaling molecule p-Erk (Figure 3, C and D).
204 Higher p-CD3ζ and p-Erk expressions in NOD $CD5^{hi}CD8^{+}$ cells compared to $CD5^{lo}CD8^{+}$
205 counterparts, consistent across TCR stimulation doses, align with the previous findings in B6 mice
206 (2, 5). The upper 5% $CD5^{hi}$ cells consistently exhibited elevated levels of T cell activation markers
207 CD69 and CD44 (Figure 3, E and F) and showed dose-dependent enhanced proliferation under

208 TCR stimulation (Figure 3G), along with their increased CD127 level (Figure 3H), suggesting
209 heightened capabilities in memory T cell homeostasis.

210 In Figure 3, C-H, we exclusively evaluated the phenotypic and functional differences
211 between $CD5^{hi}$ and $CD5^{lo}$ subsets from activated bulk $CD8^{+}$ T cells following TCR stimulation.
212 To investigate whether these distinctions post TCR activation stem from intrinsic differences
213 between $CD5^{hi}$ and $CD5^{lo}$ cells, we specifically sorted the upper and lower 10% of CD5-expressing
214 $CD8^{+}$ T cells from prediabetic NOD mice aged 6 to 8 weeks, aiming to ascertain whether sorted
215 naive $CD5^{hi}$ and $CD5^{lo}$ T cells maintain these intrinsic differences in their immune responses after
216 TCR or downstream signaling stimulation (Figure 3, I-K). The results revealed that $CD5^{hi}$ cells,
217 after TCR stimulation, displayed increased levels of the T cell activation marker CD69 (Figure 3I),
218 accompanied by higher Ki-67 expression and IFN-γ production (Figure 3J), reflecting their
219 intrinsic distinctions in heightened effector and proliferation functions. Notably, in our T cell
220 stimulation experiment comparing $CD5^{hi}$ and $CD5^{lo}CD8^{+}$ T cells treated with anti-CD3/CD28
221 dynabeads, we observed superior activation potential in $CD5^{hi}$ cells (Figure 3I). After 4 hours of
222 stimulation, CD69 expression in $CD5^{hi}$ cells was significantly higher than in $CD5^{lo}$ cells, with a
223 sharp distinction. As the stimulation time extended to 24 hours, CD69 levels in $CD5^{hi}$ compared
224 to $CD5^{lo}$ remained higher, although the difference reduced, and CD69 expression in both
225 populations became closer. In comparison, with PMA/Ionomycin treatment bypassing TCR
226 signaling initiation, there were almost no distinctions in CD69 levels between $CD5^{hi}$ and $CD5^{lo}$
227 populations, implying cell activation differences between $CD5^{hi}$ and $CD5^{lo}CD8^{+}$ T cells primarily
228 through TCR-proximal signaling. The DNA analog [methyl-3H] thymidine incorporation assay
229 further confirmed the heightened proliferation capacity in $CD5^{hi}$ subset compared to $CD5^{lo}$ subset
230 (Figure 3K). Additionally, we compared CD5 levels between $CD8^{+}CD69^{+}$ and $CD8^{+}CD69^{-}$

231 populations in both the spleen and PLNs. In PLNs, a lymphoid tissue enriched with autoantigens,
232 $CD69^{+}CD8^{+}$ T cells were skewed toward expressing higher CD5 levels compared to the
233 counterparts in spleen (Figure 3L), implying that cells with high CD5 level display elevated
234 activation potential upon encountering antigen. In summary, these results indicate that
235 diabetogenic $CD8^{+}$ T cells exhibiting increased activation and proliferation profiles in NOD mice
236 tend to have elevated CD5-associated auto-immune responses.
237

238 **The CD5 expression level in naïve $CD8^{+}$ T cells is positively correlated with**
239 **diabetes susceptibility in NOD mice.**

240 We further explored potential differences in *in vivo* immune response of $CD5^{hi}$ versus
241 $CD5^{lo}CD8^{+}$ T cells, especially their abilities to induce insulitis and diabetes through an adoptive
242 T cell transfer experiment in NOD model. Following the similar sorting method as in Figure 3, I-
243 K, the naïve $CD5^{hi}CD8^{+}$ and $CD5^{lo}CD8^{+}$ cells from prediabetic NOD mice were then administered
244 separately to immunodeficient NOD $Rag1^{-/-}$ recipients via intraperitoneal injection. The diabetes
245 incidence in $Rag1^{-/-}$ mice was weekly monitored after transfer. Strikingly, the $CD5^{hi}$-transferred
246 group exhibited markedly greater diabetes onset kinetics compared to $CD5^{lo}$ group, with the
247 appearance of diabetes as early as 4 weeks post-transfer. All 10 mice in $CD5^{hi}$ group experienced
248 earlier diabetes onset, in contrast to the $CD5^{lo}$-transferred group, where only 4 out of 11 mice
249 exhibited diabetes after approximately 20 weeks post-transfer (Figure 4A, left panel). Moreover,
250 histological analysis and insulitis scoring of pancreata after the 4-week transfer period revealed
251 heightened severity of insulitis, characterized by profound lymphocytic infiltration in the
252 $CD5^{hi}CD8^{+}$ compared to $CD5^{lo}CD8^{+}$ group (Figure 4A, right panel). This suggests that

253 $CD5^{hi}CD8^{+}$ cells possess more potent diabetogenic properties during the immune responses in
254 autoimmune diabetes.

255 Moreover, flow cytometry analysis revealed a significant increase in both the percentage
256 and the number of CD8 T cells in the spleen and PLNs of the $CD5^{hi}$-transferred group compared
257 to their $CD5^{lo}$ counterparts (Figure 4B), implying superior *in vivo* proliferation by the $CD5^{hi}$ subset,
258 consistent with the observations in *in vitro* proliferation assay (Figure 3K). Additionally, the $CD5^{hi}$
259 group exhibited higher percentages of $CD8^{+}$ T cells producing TNF-α, IFN-γ and IL-2 (Figure 4C)
260 and cells expressing the transcription factors T-bet, Eomes and the cytotoxic molecule Granzyme
261 B (Figure 4D). In characterizing other key immune markers between $CD5^{hi}$ and $CD5^{lo}$ groups, as
262 shown in Figure 1, E and F, we observed that $CD5^{hi}$ cells-transferred group in PLNs exhibited high
263 level of CD122 but not in spleen, while also maintaining high CD5 expression (Figure 4E).
264 Furthermore, we assessed the composition of central memory T cells, defined by the
265 $CD44^{hi}CD62L^{hi}$ phenotype, and quantified the percentages of $CD8^{+}$ T cells that recognize islet-
266 specific antigen $IGRP_{206–214}$ by tetramer staining ($IGRP^{+}CD8^{+}$ T cells) in the PLNs (Figure 4F).
267 This analysis underscores that central memory T cell population and the frequency of islet
268 autoantigen-specific CD8 T cells are higher in the $CD5^{hi}$ subset within the PLNs, implying more
269 robust immune responses initiated by the $CD5^{hi}$ cells.

270

271 **The intrinsic high CD5-linked self-reactivity of $CD8^{+}$ T cells attributed to**
272 **thymic positive selection contributes to the peripheral poised autoimmune**
273 **phenotypes.**

274 Based on our results, phenotypic and functional heterogeneity was observed within naive
275 $CD8^{+}$ T cells with different CD5 level (Figure 1 and 2), and the further sorted $CD5^{hi}$ and $CD5^{lo}$

276 cells displayed differential effector/memory functions (Figure 3 and 4). To validate that the
277 differential autoimmune T cell responses in $CD5^{hi}$ and $CD5^{lo}CD8^{+}$ T cells are linked to
278 heterogeneity in TCR self-reactivity during positive selection, we examined whether the unique
279 TCR basal signal strength and IL-2 production differs in the lower and upper CD5-expressing
280 thymocytes in NOD mice. Indeed, from the immature $CD4^{-}CD8^{-}$ double-negative (DN),
281 $CD4^{+}CD8^{+}$ double-positive (DP), to $CD4^{-}CD8^{+}$ (CD8SP) stages in 6-8-week-old NOD
282 thymocytes, the high self-reactivity $CD5^{hi}$ thymocytes exhibited elevated p-CD3ζ, p-Erk and IL-2
283 expression, supporting their characteristics of survival and proliferation (Figure 5A and
284 Supplementary Figure 3, A and B). These findings are consistent with previous report (2) and may
285 explain a higher $CD8^{+}$ T cell expansion observed in $CD5^{hi}CD8^{+}$ cell-transferred recipients
286 compared to $CD5^{lo}CD8^{+}$ cell-transferred recipients in the adoptive transfer experiment (Figure 4B).
287 We further explored the potential influence of thymic selection on peripheral T cell responses by
288 using the islet antigen-specific 8.3 TCR transgenic NOD8.3 mice, characterized by higher CD5
289 expression, compared to that of NOD mice, and thus an enhanced level of self-recognition.
290 NOD8.3 compared to NOD mice consistently showed elevated CD5 expression from DP to
291 CD8SP stages (Figure 5B), and a significant increase in cell number in the CD8SP subset
292 (Supplementary Figure 3, A and C), suggesting an elevated positive selection in NOD8.3
293 thymocytes. NOD8.3 mice, with elevated CD5 expression linked to basal TCR signal strength (10),
294 showed significantly higher p-CD3ζ level in DP cells compared to NOD mice counterparts (Figure
295 5C and Supplementary Figure 3D). The increase of p-CD3ζ level in DP cells positively correlates
296 with the alterations in thymocyte development reflected in increased cell number and percentage
297 in the CD8SP subset transitioning from the DP stage of NOD8.3 mice (Figure 5D and
298 Supplementary Figure 3C). Additionally, DN thymocytes, marked by CD44 and CD25, undergo

299 crucial β-selection in DN3 ($CD44^{-}CD25^{+}$) and DN4 ($CD44^{-}CD25^{-}$), emphasizing the importance
300 of DN stage in thymocyte development (48-51). NOD8.3 mice showed significantly higher cell
301 numbers in DN4 (Figure 5E and Supplementary Figure 3E), suggesting a selection advantage in
302 these stages due to bypassing the need for TCRβ rearrangement occurred in NOD cells.

303 Positive selection in the DP stage was further characterized by analyzing CD69 and TCRβ
304 levels. In the pre-positive selection population (DP/$TCR\beta^{-}CD69^{-}$), NOD8.3 cells showed
305 significantly higher CD5 expression compared to NOD cells (Figure 5F, upper panel, and
306 Supplementary Figure 3F), implying an enhanced TCR signal perception at the initiation of DP
307 positive selection (52). Consistently, the frequency of $CD69^{+}TCR\beta^{+}$ cells, representing post-
308 positive-selection thymocytes (53), significantly increased in NOD8.3 compared to NOD mice
309 (Figure 5F, lower panel), predisposing to an accelerated accumulation of CD8SP cells (Figure 5D
310 and Supplementary Figure 3C). Additionally, to investigate whether the increased accumulation
311 of CD8SP cell number in NOD8.3 mice is associated with elevated expressions of cytokine
312 receptors crucial for T cell survival in DP stage, we assessed the expression levels of CD122,
313 CD127, CD44 and CD25 in DP thymocytes. Indeed, these receptors showed higher levels in
314 NOD8.3 compared to NOD DP thymocytes (Figure 5G), suggesting their contribution to cell
315 survival into the CD8SP stage. Remarkably, NOD8.3 mice showed an increased percentage of
316 memory-like $CD122^{hi}CD44^{hi}$ cells (V_M; virtually memory) in CD8SP compared to NOD mice
317 (Figure 5H and Supplementary Figure 3G), implying a direct transition to memory T cells upon
318 entering peripheral tissues (54). Furthermore, CD5 expression patterns were compared across
319 thymocyte stages among different NOD strains including NOD, BDC2.5 and NOD8.3 mice.
320 NOD8.3 thymocytes consistently showed higher CD5 levels compared to two other strains from
321 the DN to DP stages, and notably, in the CD8SP stage, NOD8.3 cells exhibited the highest CD5

322 expression, followed by NOD and then BDC2.5 cells (Supplementary Figure 4A). Interestingly,
323 NOD8.3 cells displayed enhanced proliferation (Supplementary Figure 4, B and C), suggesting a
324 potential link between perceived TCR basal signals during thymocyte selection and peripheral
325 lymphocyte proliferation.
326

327 Downregulation of TCR signaling strength by transgenic phosphatase Pep 328 expression does not confer the protection in dLPC/NOD8.3 mice.

329 Based on the insights gained from thymocyte development in NOD, BDC2.5 and NOD8.3
330 mice, where the TCR signal strength influences intrinsic T cell response and subsequent effector
331 function, we investigated whether the manipulation on TCR basal signal strength influences
332 autoimmune potential of peripheral T cells in NOD mice. To address this issue, we utilized two
333 transgenic mouse model, dLPC/NOD and dLPE/NOD mice, which express a T cell-specific
334 phosphatase Pep to downregulate proximal TCR signaling (27). A significant decrease in
335 autoimmune diabetes, in terms of a delayed onset, less insulitis severity and lower incidence of
336 disease, was found in dLPC/NOD and dLPE/NOD mice compared to NOD controls (27). As
337 expected, transgenic Pep expression in dLPC/NOD mice delayed the onset of diabetes and reduced
338 insulitis. However, Pep overexpression in dLPC/NOD8.3 mice did not provide protection (Figure
339 6A), suggesting that intrinsic high CD5-associated self-reactivity in NOD8.3 T cells overrides the
340 transgenic Pep-mediated protection observed in dLPC/NOD mice. Moreover, overexpression of
341 Pep in dLPC/NOD and dLPC/NOD8.3 mice did not change the CD5 expression of T cells in the
342 spleen compared to their controls, NOD and NOD8.3, respectively. Interestingly, we observed a
343 transgenic Pep-mediated CD5 downregulation in $CD8^+$ T cells in PLNs, enriched with islet-
344 specific autoantigens, of dLPC/NOD mice compared to NOD controls (Figure 6B), suggesting that

345 the transgenic Pep-mediated TCR signaling strength modulates CD5 expression in a context-
346 specific manner. However, CD5 expression level in $CD8^+$ T cells in PLNs of dLPC/NOD8.3 was
347 similar to NOD8.3 mice (Figure 6B), suggesting that NOD8.3 T cells with an intrinsic high CD5-
348 associated self-reactivity are more resistant to transgenic Pep-mediated change in TCR signaling
349 and CD5 expression. These observations are further supported by our data that the CD5-correlated
350 basal TCR signaling molecule, p-CD3ζ, was attenuated in dLPC/NOD mice but not in
351 dLPC/NOD8 .3 mice, both in the spleen and PLNs (Figure 6C). Collectively, our results suggest
352 that $CD8^+$ T cells with intrinsic high CD5-linked self-reactivity are more resistant to transgenic
353 Pep-mediated TCR signaling downregulation and sustain the diabetogenic susceptibility in
354 NOD8.3 mice.

355 Consistently, isolated naïve $CD8^+$ T cells (Supplementary Figure 5 A, left panel) from high
356 CD5-expressing NOD8.3 mice exhibited superior proliferation compared to cells from NOD mice
357 upon anti-CD3/CD28 or PMA/Iono stimulation (Supplementary Figure 5A, middle and right panel,
358 respectively). Moreover, transgenic Pep expression attenuated $CD8^+$ T cell proliferation in both
359 dLPC/NOD and dLPE/NOD mice compared to NOD controls (Supplementary Figure 5B).
360 However, transgenic Pep expression did not alter cell proliferation in dLPE/NOD8.3 T cells when
361 stimulated with the autoantigen-specific self-peptide $IGRP_{206-214}$ (Supplementary Figure 5C),
362 suggesting that a high TCR basal signal conferred by elevated intrinsic self-reactivity overrides
363 the transgenic Pep-mediated reduction of T cell proliferation. Further analysis of p-Erk level also
364 showed a significant decrease in dLPC/NOD compared to NOD mice. Similarly, transgenic Pep
365 did not attenuate the p-Erk level in dLPC/NOD8.3 mice (Figure 6D), consistent with the
366 observation of p-CD3ζ level in these Pep transgenic mice (Figure 6C). Additionally, CD69 and
367 KLRG1 (Figure 6E) and other activation markers including CD44 and CXCR3 (Supplementary

368 Figure 5D) were decreased in dLPC/NOD or dLPE/NOD mice compared to NOD controls. Similar
369 to previous observations, transgenic Pep-mediated attenuation of T cell activation was abolished
370 in dLPC/NOD8.3 mice, supporting again that an intrinsic high CD5-linked self-reactivity is able
371 to confer the impact by transgenic Pep-mediated TCR signaling change.

372 In addition, transgenic Pep expression downregulated CD25 level in T cells of PLNs, not
373 in spleen, in dLPC/NOD mice compared to NOD mice, whereas there was no significant change
374 in CD25 expression between dLPC/NOD8.3 and NOD8.3 mice (Figure 6F). Moreover, memory
375 T cell homeostasis molecules, such as CD122 and CD44, were also reduced in T cells of PLNs,
376 not in spleen, in dLPC/NOD mice compared to NOD mice (Figure 6F and Supplementary Figure
377 5D), but were indistinguishable between dLPC/NOD8.3 and NOD8.3 mice (Figure 6F). Notably,
378 transgenic Pep expression in dLPC/NOD mice significantly reduced production of effector T cell
379 cytokines, such as IL-2, TNF-α and IFN-γ in $CD8^+$ T cells compared to NOD mice (Figure 6G and
380 Supplementary Figure 5E). Nevertheless, transgenic Pep-mediated reduction in cytokine
381 production was abolished in dLPC/NOD8.3 mice (Figure 6G). Collectively, our results indicate
382 that CD5-associated high self-reactivity is able to abolish transgenic Pep-mediated attenuation of
383 effector/memory T cell functions in NOD8.3 mice.

384

385 **Analysis of the $CD5^{hi}$ population identifies TCR repertoires associated with**
386 **autoimmune diseases.**

387 To investigate whether pathogenic feature in $CD5^{hi}CD8^+$ population reflects in their TCR
388 repertoire, we divided naïve $CD8^+$ T cells into $CD5^{hi}CD8^+$ and $CD5^{lo}CD8^+$ groups, conducted bulk
389 RNA sequencing on two groups, and applied the MiXCR pipeline to analyze TCR repertoire
390 composition in $CD5^{hi}$ and $CD5^{lo}$ groups (Figure 7A and Supplementary Figure 6). Analysis of T-

391 cell receptor-α chain (*TRAV* and *TRAJ*) and T-cell receptor-β chain (*TRBV* and *TRBJ*) gene usages
392 in $CD5^{hi}CD8^{+}$ and $CD5^{lo}CD8^{+}$ T cells revealed increased utilization of *TRAV13-2*, *TRAV16D-*
393 *DV11*, *TRAV3-3*, *TRAJ32*, *TRBV14*, *TRBV16*, *TRBJ2-1* and *TRBJ2-7* in $CD5^{hi}CD8^{+}$ cells, with the
394 exception of *TRAV9-1*, which exhibited lower utilization in $CD5^{hi}CD8^{+}$ T cells (Figure 7, B-E).
395 The CDR3 loops of TRA (CDR3α) and TRB (CDR3β), crucial for antigen recognition by TCRs
396 on T cells, are shaped by the diverse recombination events that assemble TRA VJ gene segments
397 and TRB V(D)J gene segments (55). The distinct utilization of V or J gene families of TCRα and
398 TCRβ, as shown in Figure 7, B-E, may lead to variable CDR3 characteristics between $CD5^{hi}CD8^{+}$
399 and $CD5^{lo}CD8^{+}$ T cells. Additionally, emerging evidence suggests a potential association of
400 shorter CDR3 length in T1D patients (56). Therefore, we analyzed whether the $CD5^{hi}CD8^{+}$ cells
401 have similar pathogenic CDR3 patterns. Interestingly, examination of CDR3α and CDR3β length
402 distribution in the TCR repertoire revealed a bias toward shorter length in the $CD5^{hi}$ compared to
403 the $CD5^{lo}$ group, particularly with a significantly shorter CDR3β length (Figure 7F). Shared TCR
404 pools were reported to be enriched in clonotypes with fewer insertions in CDR3 (57). To confirm
405 this, the overlapped clonal count matrix for CDR3α or CDR3β motif was calculated among all
406 groups (Figure 7G), indicating increased similarity between the $CD5^{hi}$ groups based on its own
407 pairing comparison. Strikingly, the IGRP-recognizing CDR3 motif was found in CDR3α of the
408 $CD5^{hi}$ group (Figure 7H), which has been identified in the TCR repertoire of T1D patients (58).
409 Moreover, analysis of CDR3α and CDR3β amino acid characteristics revealed a hydrophobicity
410 enrichment in TRA of $CD5^{hi}CD8^{+}$ cells (Figure 7I), consistent with a previous study demonstrating
411 that the generation of high self-reactive T cells was promoted by hydrophobic residues within the
412 CDR3 region (59). Furthermore, in alignment with a previous study illustrating greater diversity
413 in TCR repertoires from T1D patients than in healthy donors (56), $CD5^{hi}CD8^{+}$ cells exhibited

414 higher diversity in clonotypes compared to their $CD5^{lo}$ counterpart (Figure 7J). Additionally, our
415 results align with a previous study that employed high-throughput TCR-seq analyses in mice,
416 identifying highly shared CDR3 sequences among mice characterized by restricted V and J
417 segment usage (60). These CDR3 sequences, exhibiting lower nucleotide insertions and shorter
418 lengths, were more abundant, particularly in individuals displaying autoimmune and allograft-
419 related reactions, further affirming their association with self-antigen reactivity. In conclusion,
420 these results suggest that $CD5^{hi}CD8^{+}$ T cells, with elevated self-reactivity and increased clonal
421 diversity, are intrinsically linked to the utilization of specific V and J genes within $CD5^{hi}$ cells.
422
423
424
425
426
427
428
429
430
431
432
433
434

435 **Discussion**

436 In our study, $CD5^{hi}CD8^{+}$ T cells, with heightened basal signals and increased self-ligand
437 reactivity, show enhanced avidity for the autoantigen IGRP (Figure 8). These cells transition
438 quickly into effector/memory cells upon encountering autoantigens, expressing markers like CD69
439 and CD44. Activation via CD122 and CD127 promotes cytokine secretion, contributing to
440 inflammation and β cell destruction. Further investigation is needed to understand the role of these
441 memory-like $CD8^{+}$ T cells in autoreactivity. The loss of Pep-conferred protection in high CD5-
442 expressing NOD8.3 mice highlights the significance of elevated TCR basal signals from positive
443 selection in autoimmune responses, suggesting potential targets for treating T1D and related
444 disorders.

445 In contrast to previous studies that compared TCR signaling in NOD and wild-type B6
446 mice (11), we investigate how thymic self-recognition impacts TCR signal strength and $CD8^{+}$ T
447 cell pathogenicity in NOD mice. Our research also differs from studies focusing on the
448 $CD4^{+}CD5^{low}$ T-cell population (12), which resembles central memory T cells and is linked to
449 spontaneous autoimmunity in NOD mice. Instead, we find distinct TCR signal strength variations
450 between $CD5^{hi}$ and $CD5^{lo}$ cells, with $CD5^{hi}CD8^{+}$ cells showing enhanced activation, proliferation
451 and disease transfer potential. This discrepancy may arise from the higher CD5-expressing
452 distribution in the naïve $CD4^{+}$ T cells compared to the naïve $CD8^{+}$ T cells, suggesting distinct TCR
453 signaling sensitivity when stimulated and resulting in different functional activation thresholds
454 between $CD4^{+}$ and $CD8^{+}$ T cells (61, 62). Our results reveal that $CD5^{hi}CD8^{+}$ T cells exhibit
455 elevated CD25 and CD122 expression compared to their $CD5^{lo}CD8^{+}$ counterparts, indicating
456 increased sensitivity to IL-2 stimulation. While exposure to IL-2 may enhance cell expansion in
457 $CD8^{+}$ cells, it can lead to overstimulation in $CD4^{+}$ T cells, resulting in activation-induced cell death.

458 Surprisingly, clinical cases of type 1 diabetes reflect similar findings to our animal mouse model
459 study. Children with T1D exhibit higher CD5 expression in $CD8^+$ T cells compared to healthy
460 controls (63). These observations underscore the complexity of immune responses in autoimmune
461 diseases and warrant further exploration to unravel the underlying mechanisms and hold promise
462 for therapeutic interventions in autoimmune diseases.

463 Nevertheless, the role of CD5 itself in shaping the distinctive functions of $CD5^{hi}$ and $CD5^{lo}$
464 cells remains largely unclear (64, 65). A previous research has indicated that CD5 serves as a
465 scaffold protein, retaining the NF-κB inhibitor IκBα in the cytosol to prevent its inhibition of NF-
466 κB signaling (66), though studies of $Cd5^{-/-}$ mice do not appear to support this concept (67). This
467 mechanism confers survival advantages to $CD5^{hi}$ T cells. This observation may help elucidate the
468 seemingly paradoxical result that CD5's primary function is to attenuate TCR-proximal signaling;
469 however interestingly, antigen-specific T cells with higher initial CD5 expression exhibit enhanced
470 persistence as effector/memory cells following a peripheral challenge. Whether $CD5^{hi}CD8^+$ T cells
471 execute potent autoimmune responses through the modulation of NF-κB-dependent signaling
472 needs further investigation.

473 Exploring how TCR composition contributes to the distinct responses between $CD5^{hi}$ and
474 $CD5^{lo}$ cells is beyond the scope of our study. Nonetheless, prior research, which involved screening
475 autoimmune disease databases such as arthritis, diabetes, etc., has revealed a trend in specific TCR
476 repertoire usage characterized by germline-encoded TCRs with fewer nucleotide insertions and
477 shorter CDR3 length (60). It is consistent with our results, demonstrating that $CD5^{hi}$ T cells,
478 skewed toward shorter CDR3 lengths in the TCR repertoire, have a higher potential for
479 autoreactivity. Consequently, the high self-pMHC reactivity of T cells provides a stronger TCR
480 basal signal, potentially priming T cells with specific TCR compositions for robust responses to

481 foreign antigens in the future. From an evolutionary perspective, this TCR design may have
482 initially conferred an advantage by enhancing immune responses against pathogen infections.
483 However, it might have come at the cost of an increased risk of autoimmune diseases. A previous
484 study explored the TCR repertoire of $CD8^+$ T cells recognizing the islet-specific peptide $IGRP_{206–}$
485 $_{214}$ in both grafted and endogenous islet infiltrates, revealing a shared repertoire favoring specific
486 gene segments and limited diversity and clonotypic expansion within $IGRP_{206–214}$-specific $CD8^+$
487 T cells in NOD mice (58). Another study of effector/memory $CD4^+$ and $CD8^+$ T cells involved in
488 autoimmune rejection of islet grafts in diabetic NOD mice demonstrated a comparable pattern of
489 TCR repertoire diversity (68). Our analysis of TCR gene usage in $CD5^{hi}CD8^+$ and $CD5^{lo}CD8^+$ T
490 cells also revealed distinct patterns, suggesting potential functional differences between these
491 subsets. The identified differences included increased usage of TRAV13-2, TRAV16D-DV11,
492 TRAV3-3, TRAJ32, TRBV14, TRBV16, TRBJ2-1, and TRBJ2-7 in $CD5^{hi}$ compared to $CD5^{lo}$
493 cells, while TRAV9-1 was reduced in $CD5^{hi}$ cells. Notably, previous studies identified specific
494 gene segments associated with autoimmune diseases like Sjögren's syndrome (TRAV13-2) (69),
495 inflammatory bowel disease, ulcerative colitis (TRBJ2-1 and TRBJ2-7) (70, 71), and type 1
496 diabetes (TRBV14 and TRBV16) (72), underscoring the importance of understanding T-cell
497 receptor dynamics in autoimmune pathogenesis across various disorders.

498 Several studies have highlighted the impact of TCR-self-pMHC interactions during
499 positive selection on signaling molecules' localization, such as p-Erk, particularly in B cells and
500 $CD4^+$ T cells (4, 73, 74). Similarly, our $CD5^{hi}CD8^+$ T cells may consistently receive stronger
501 signals, leading to better synchronization and activation of Erk at the cell membrane. However,
502 despite using PMA/Iono to bypass proximal TCR signaling and elicit downstream responses,
503 differences in T cell proliferation response persisted between $CD5^{hi}$ and $CD5^{lo}$ or between NOD

504 and NOD8.3 $CD8^+$ T cells. This suggests that TCR-self-peptide interaction influences T cells
505 beyond just proximal TCR signaling intensity. There may be pre-existing transcriptional
506 differences influenced by genes involved in T-cell receptor signaling established during thymic
507 development among naïve NOD $CD8^+$ T cells, affecting their effector lineage fate (75).
508 Additionally, in a previous experimental autoimmune diabetes model, OVA antigen-specific $CD8^+$
509 T cells with a virtual memory phenotype and high CD5 expression showed a low capacity to induce
510 diabetes (76), contrasting with the pathogenic features of our $CD5^{hi}CD8^+$ cells. This suggests that
511 naïve $CD5^{hi}CD8^+$ T cells in NOD mice may only partially resemble virtual memory T cells, posing
512 intriguing questions requiring further investigation.
513
514
515
516
517
518
519
520
521
522
523
524
525

526 ## Materials and methods

527 *Mice*. The mice utilized in this study included NOD/Sytwu, NOD8.3, and NOD.BDC2.5 TCR
528 transgenic mice, alongside Ptpn22-transgenic NOD mice, designated dLck–Ptpn22 C (dLPC/NOD)
529 and dLck–Ptpn22 E (dLPE/NOD), previously generated by cloning Ptpn22 from NOD mouse
530 splenocytes and microinjecting it into single-cell NOD embryos. The resulting dLck–Ptpn22
531 transgenic mice were genotyped by PCR and evaluated by Southern blot analysis for confirmation.
532 Western blot analysis revealed the expression of transgenic Pep in thymocytes and splenic T cells
533 of dLPC and dLPE mice, with a stepwise increase in Pep protein levels from nontransgenic
534 littermates, dLPC/NOD to dLPE/NOD mice (27). The transgenic mice dLPC/NOD, dLPE/NOD,
535 dLPC/NOD8.3 and dLPE/NOD8.3 used in the study were hemizygous for the Ptpn22 transgene
536 (Supplementary Figure 7). dLPC/NOD8.3 and dLPE/NOD8.3 were established by mating
537 dLPC/NOD or dLPE/NOD mice with NOD8.3 mice. NOD/Sytwu, NOD8.3 and NOD.BDC2.5
538 TCR transgenic mice were originally obtained from The Jackson Laboratory, while NOD/Rag1$^{-/-}$
539 mice were procured from the National Laboratory Animal Center. The study adhered to
540 institutional guidelines and was approved by the National Defense Medical Center Institutional
541 Animal Care and Use Committee.

542 *Sex as a biological variable.* Our study exclusively examined female mice because the disease
543 modeled is relevant in females.

544 *Statistics.* The log-rank (Mantel–Cox) test was employed for survival curve comparisons. Two-
545 group comparisons utilized a 2-tailed Student's unpaired t-test, two-sample comparison utilized

546 Welch two sample t-test, and multigroup comparisons utilized one-way ANOVA with Tukey's
547 post-test. A significance level of $P < 0.05$ was considered significant.

548 *Study approval*. All protocols involving live animals adhered to institutional guidelines and
549 received approval from the Institutional Animal Care and Use Committee at the National Defense
550 Medical Center (Taipei, Taiwan).
551
552 Additional methods can be found in the Supplementary Material.
553
554 *Supplementary material.* Supplementary material provided with this study includes Supplementary
555 Figures 1-7, Supplementary Tables 1-6 and Supplementary methods.
556

557 **Data availability**

558 The TCR repertoires of $CD5^{hi}$ and $CD5^{lo}$, along with the data analyzed using R and the
559 corresponding codes, are available in the following GitHub repository: https://github.com/Chia-
560 Lo/TCR-signal-strength-modulates-antigen-specific-CD8-T-cell-pathogenicity-in-non-obese-
561 diabetic-mice.git
562
563
564
565
566
567

568 **Author contributions**

569 CLH and LTY performed experiments and analyzed data. CLH, LTY, YWL and JLD performed
570 experiments. LTY gave advice. CLH and HKS wrote the manuscript.

571

572 **Acknowledgments**

573 This work was supported by the Ministry of Science and Technology of the Republic of China
574 (MOST 109-2320-B-400-018-MY3, MOST 110-2320-B-400-011-MY3), National Science and
575 Technology Council (NSTC 112-2320-B-400-026-MY3) and Tri-Service General Hospital
576 (TSGH-C02-112029, TSGH-C03-113037, VTA112-T-1-1, VTA113-T-1-1). The authors
577 acknowledge the technical services provided by Instrument Center of National Defense Medical
578 Center.

579

580 **Abbreviations**

581 dLPC/NOD, *Lck* distal promoter– *Ptpn22* C line in NOD background; dLPE/NOD, *Lck* distal
582 promoter– *Ptpn22* E line in NOD background. NOD, non-obese diabetic.

583

584

585

586

587

588

589

590

591 **References**

592 1. Gascoigne NR, Rybakin V, Acuto O, and Brzostek J. TCR Signal Strength and T Cell
593 Development. *Annu Rev Cell Dev Biol.* 2016;32:327-48.
594 2. Persaud SP, Parker CR, Lo WL, Weber KS, and Allen PM. Intrinsic CD4+ T cell sensitivity
595 and response to a pathogen are set and sustained by avidity for thymic and peripheral
596 complexes of self peptide and MHC. *Nat Immunol.* 2014;15(3):266-74.
597 3. Fulton RB, Hamilton SE, Xing Y, Best JA, Goldrath AW, Hogquist KA, et al. The TCR's
598 sensitivity to self peptide-MHC dictates the ability of naive CD8(+) T cells to respond to
599 foreign antigens. *Nat Immunol.* 2015;16(1):107-17.
600 4. Myers DR, Zikherman J, and Roose JP. Tonic Signals: Why Do Lymphocytes Bother?
601 *Trends Immunol.* 2017;38(11):844-57.
602 5. Mandl JN, Monteiro JP, Vrisekoop N, and Germain RN. T cell-positive selection uses self-
603 ligand binding strength to optimize repertoire recognition of foreign antigens. *Immunity.*
604 2013;38(2):263-74.
605 6. Deshpande NR, Parrish HL, and Kuhns MS. Self-recognition drives the preferential
606 accumulation of promiscuous CD4(+) T-cells in aged mice. *Elife.* 2015;4:e05949.
607 7. Sadigh S, Scott BB, Mageed RA, Malcolm A, Andrew EM, and Maini RN. Identification of
608 hybridomas derived from mouse CD5+ B lymphocytes by fluorescent staining for
609 cytoplasmic CD5 expression. *Immunology.* 1994;81(4):558-63.
610 8. Tarakhovsky A, Kanner SB, Hombach J, Ledbetter JA, Muller W, Killeen N, et al. A role
611 for CD5 in TCR-mediated signal transduction and thymocyte selection. *Science.*
612 1995;269(5223):535-7.

613 9. Perez-Villar JJ, Whitney GS, Bowen MA, Hewgill DH, Aruffo AA, and Kanner SB. CD5
614 negatively regulates the T-cell antigen receptor signal transduction pathway: involvement of
615 SH2-containing phosphotyrosine phosphatase SHP-1. *Mol Cell Biol.* 1999;19(4):2903-12.
616 10. Azzam HS, Grinberg A, Lui K, Shen H, Shores EW, and Love PE. CD5 expression is
617 developmentally regulated by T cell receptor (TCR) signals and TCR avidity. *J Exp Med.*
618 1998;188(12):2301-11.
619 11. Dong M, Audiger C, Adegoke A, Lebel ME, Valbon SF, Anderson CC, et al. CD5 levels
620 reveal distinct basal T-cell receptor signals in T cells from non-obese diabetic mice. *Immunol*
621 *Cell Biol.* 2021.
622 12. Kong Y, Jing Y, Allard D, Scavuzzo MA, Sprouse ML, Borowiak M, et al. A dormant T-
623 cell population with autoimmune potential exhibits low self-reactivity and infiltrates islets
624 in type 1 diabetes. *Eur J Immunol.* 2022.
625 13. Lutes LK, Steier Z, McIntyre LL, Pandey S, Kaminski J, Hoover AR, et al. T cell self-
626 reactivity during thymic development dictates the timing of positive selection. *Elife.* 2021;10.
627 14. Han B, Serra P, Yamanouchi J, Amrani A, Elliott JF, Dickie P, et al. Developmental control
628 of CD8 T cell-avidity maturation in autoimmune diabetes. *J Clin Invest.* 2005;115(7):1879-
629 87.
630 15. Amrani A, Verdaguer J, Serra P, Tafuro S, Tan R, and Santamaria P. Progression of
631 autoimmune diabetes driven by avidity maturation of a T-cell population. *Nature.*
632 2000;406(6797):739-42.
633 16. Mingueneau M, Jiang W, Feuerer M, Mathis D, and Benoist C. Thymic negative selection
634 is functional in NOD mice. *J Exp Med.* 2012;209(3):623-37.

635 17. Eisenbarth GS. Type I diabetes mellitus. A chronic autoimmune disease. *N Engl J Med.*
636 1986;314(21):1360-8.
637 18. Ziegler AG, and Nepom GT. Prediction and pathogenesis in type 1 diabetes. *Immunity.*
638 2010;32(4):468-78.
639 19. Herold KC, Vignali DA, Cooke A, and Bluestone JA. Type 1 diabetes: translating
640 mechanistic observations into effective clinical outcomes. *Nat Rev Immunol.*
641 2013;13(4):243-56.
642 20. Pearson JA, Wong FS, and Wen L. The importance of the Non Obese Diabetic (NOD) mouse
643 model in autoimmune diabetes. *J Autoimmun.* 2016;66:76-88.
644 21. Anderson MS, and Bluestone JA. The NOD mouse: a model of immune dysregulation. *Annu*
645 *Rev Immunol.* 2005;23:447-85.
646 22. Fousteri G, Liossis SN, and Battaglia M. Roles of the protein tyrosine phosphatase PTPN22
647 in immunity and autoimmunity. *Clin Immunol.* 2013;149(3):556-65.
648 23. Ivashkiv LB. PTPN22 in autoimmunity: different cell and different way. *Immunity.*
649 2013;39(1):91-3.
650 24. Bottini N, and Peterson EJ. Tyrosine phosphatase PTPN22: multifunctional regulator of
651 immune signaling, development, and disease. *Annu Rev Immunol.* 2014;32:83-119.
652 25. Verdaguer J, Yoon JW, Anderson B, Averill N, Utsugi T, Park BJ, et al. Acceleration of
653 spontaneous diabetes in TCR-beta-transgenic nonobese diabetic mice by beta-cell cytotoxic
654 CD8+ T cells expressing identical endogenous TCR-alpha chains. *J Immunol.*
655 1996;157(10):4726-35.

656 26. Verdaguer J, Schmidt D, Amrani A, Anderson B, Averill N, and Santamaria P. Spontaneous
657 autoimmune diabetes in monoclonal T cell nonobese diabetic mice. *J Exp Med.*
658 1997;186(10):1663-76.
659 27. Yeh LT, Miaw SC, Lin MH, Chou FC, Shieh SJ, Chuang YP, et al. Different modulation of
660 Ptpn22 in effector and regulatory T cells leads to attenuation of autoimmune diabetes in
661 transgenic nonobese diabetic mice. *J Immunol.* 2013;191(2):594-607.
662 28. Kaech SM, and Cui W. Transcriptional control of effector and memory CD8+ T cell
663 differentiation. *Nat Rev Immunol.* 2012;12(11):749-61.
664 29. Pearce EL, Mullen AC, Martins GA, Krawczyk CM, Hutchins AS, Zediak VP, et al. Control
665 of effector CD8+ T cell function by the transcription factor Eomesodermin. *Science.*
666 2003;302(5647):1041-3.
667 30. Intlekofer AM, Takemoto N, Wherry EJ, Longworth SA, Northrup JT, Palanivel VR, et al.
668 Effector and memory CD8+ T cell fate coupled by T-bet and eomesodermin. *Nat Immunol.*
669 2005;6(12):1236-44.
670 31. Zhu Y, Ju S, Chen E, Dai S, Li C, Morel P, et al. T-bet and eomesodermin are required for
671 T cell-mediated antitumor immune responses. *J Immunol.* 2010;185(6):3174-83.
672 32. Lord GM, Rao RM, Choe H, Sullivan BM, Lichtman AH, Luscinskas FW, et al. T-bet is
673 required for optimal proinflammatory CD4+ T-cell trafficking. *Blood.* 2005;106(10):3432-
674 9.
675 33. Banerjee A, Gordon SM, Intlekofer AM, Paley MA, Mooney EC, Lindsten T, et al. Cutting
676 edge: The transcription factor eomesodermin enables CD8+ T cells to compete for the
677 memory cell niche. *J Immunol.* 2010;185(9):4988-92.

678 34. Palmer MJ, Mahajan VS, Chen J, Irvine DJ, and Lauffenburger DA. Signaling thresholds
679 govern heterogeneity in IL-7-receptor-mediated responses of naive CD8(+) T cells. *Immunol*
680 *Cell Biol.* 2011;89(5):581-94.
681 35. Boyman O, Letourneau S, Krieg C, and Sprent J. Homeostatic proliferation and survival of
682 naive and memory T cells. *Eur J Immunol.* 2009;39(8):2088-94.
683 36. Lenz DC, Kurz SK, Lemmens E, Schoenberger SP, Sprent J, Oldstone MB, et al. IL-7
684 regulates basal homeostatic proliferation of antiviral CD4+T cell memory. *Proc Natl Acad*
685 *Sci U S A.* 2004;101(25):9357-62.
686 37. Rubinstein MP, Lind NA, Purton JF, Filippou P, Best JA, McGhee PA, et al. IL-7 and IL-15
687 differentially regulate CD8+ T-cell subsets during contraction of the immune response.
688 *Blood.* 2008;112(9):3704-12.
689 38. Cibrian D, and Sanchez-Madrid F. CD69: from activation marker to metabolic gatekeeper.
690 *Eur J Immunol.* 2017;47(6):946-53.
691 39. Rea IM, McNerlan SE, and Alexander HD. CD69, CD25, and HLA-DR activation antigen
692 expression on CD3+ lymphocytes and relationship to serum TNF-alpha, IFN-gamma, and
693 sIL-2R levels in aging. *Exp Gerontol.* 1999;34(1):79-93.
694 40. Ahn E, Araki K, Hashimoto M, Li W, Riley JL, Cheung J, et al. Role of PD-1 during effector
695 CD8 T cell differentiation. *Proc Natl Acad Sci U S A.* 2018;115(18):4749-54.
696 41. Agata Y, Kawasaki A, Nishimura H, Ishida Y, Tsubata T, Yagita H, et al. Expression of the
697 PD-1 antigen on the surface of stimulated mouse T and B lymphocytes. *Int Immunol.*
698 1996;8(5):765-72.

699 42. Herndler-Brandstetter D, Ishigame H, Shinnakasu R, Plajer V, Stecher C, Zhao J, et al.
700 KLRG1(+) Effector CD8(+) T Cells Lose KLRG1, Differentiate into All Memory T Cell
701 Lineages, and Convey Enhanced Protective Immunity. *Immunity.* 2018;48(4):716-29 e8.
702 43. Park JH, Adoro S, Lucas PJ, Sarafova SD, Alag AS, Doan LL, et al. 'Coreceptor tuning':
703 cytokine signals transcriptionally tailor CD8 coreceptor expression to the self-specificity of
704 the TCR. *Nat Immunol.* 2007;8(10):1049-59.
705 44. Cho JH, Kim HO, Surh CD, and Sprent J. T cell receptor-dependent regulation of lipid rafts
706 controls naive CD8+ T cell homeostasis. *Immunity.* 2010;32(2):214-26.
707 45. Lovering RC, Camon EB, Blake JA, and Diehl AD. Access to immunology through the Gene
708 Ontology. *Immunology.* 2008;125(2):154-60.
709 46. Dorner BG, Dorner MB, Zhou X, Opitz C, Mora A, Guttler S, et al. Selective expression of
710 the chemokine receptor XCR1 on cross-presenting dendritic cells determines cooperation
711 with CD8+ T cells. *Immunity.* 2009;31(5):823-33.
712 47. Best JA, Blair DA, Knell J, Yang E, Mayya V, Doedens A, et al. Transcriptional insights
713 into the CD8(+) T cell response to infection and memory T cell formation. *Nat Immunol.*
714 2013;14(4):404-12.
715 48. Godfrey DI, Kennedy J, Suda T, and Zlotnik A. A developmental pathway involving four
716 phenotypically and functionally distinct subsets of CD3-CD4-CD8- triple-negative adult
717 mouse thymocytes defined by CD44 and CD25 expression. *J Immunol.* 1993;150(10):4244-
718 52.
719 49. Michie AM, and Zuniga-Pflucker JC. Regulation of thymocyte differentiation: pre-TCR
720 signals and beta-selection. *Semin Immunol.* 2002;14(5):311-23.

721 50. Yamasaki S, and Saito T. Molecular basis for pre-TCR-mediated autonomous signaling.
722 *Trends Immunol.* 2007;28(1):39-43.
723 51. Hoffman ES, Passoni L, Crompton T, Leu TM, Schatz DG, Koff A, et al. Productive T-cell
724 receptor beta-chain gene rearrangement: coincident regulation of cell cycle and clonality
725 during development in vivo. *Genes Dev.* 1996;10(8):948-62.
726 52. Fu G, Vallee S, Rybakin V, McGuire MV, Ampudia J, Brockmeyer C, et al. Themis controls
727 thymocyte selection through regulation of T cell antigen receptor-mediated signaling. *Nat*
728 *Immunol.* 2009;10(8):848-56.
729 53. Kim S, Park GY, Park JS, Park J, Hong H, and Lee Y. Regulation of positive and negative
730 selection and TCR signaling during thymic T cell development by capicua. *Elife.* 2021;10.
731 54. Miller CH, Klawon DEJ, Zeng S, Lee V, Socci ND, and Savage PA. Eomes identifies thymic
732 precursors of self-specific memory-phenotype CD8(+) T cells. *Nat Immunol.*
733 2020;21(5):567-77.
734 55. Hughes MM, Yassai M, Sedy JR, Wehrly TD, Huang CY, Kanagawa O, et al. T cell receptor
735 CDR3 loop length repertoire is determined primarily by features of the V(D)J recombination
736 reaction. *Eur J Immunol.* 2003;33(6):1568-75.
737 56. Gomez-Tourino I, Kamra Y, Baptista R, Lorenc A, and Peakman M. T cell receptor beta-
738 chains display abnormal shortening and repertoire sharing in type 1 diabetes. *Nat Commun.*
739 2017;8(1):1792.
740 57. Zvyagin IV, Pogorelyy MV, Ivanova ME, Komech EA, Shugay M, Bolotin DA, et al.
741 Distinctive properties of identical twins' TCR repertoires revealed by high-throughput
742 sequencing. *Proc Natl Acad Sci U S A.* 2014;111(16):5980-5.

743 58. Fuchs YF, Eugster A, Dietz S, Sebelefsky C, Kuhn D, Wilhelm C, et al. CD8(+) T cells
744 specific for the islet autoantigen IGRP are restricted in their T cell receptor chain usage. *Sci*
745 *Rep.* 2017;7:44661.
746 59. Stadinski BD, Shekhar K, Gomez-Tourino I, Jung J, Sasaki K, Sewell AK, et al.
747 Hydrophobic CDR3 residues promote the development of self-reactive T cells. *Nat Immunol.*
748 2016;17(8):946-55.
749 60. Madi A, Shifrut E, Reich-Zeliger S, Gal H, Best K, Ndifon W, et al. T-cell receptor
750 repertoires share a restricted set of public and abundant CDR3 sequences that are associated
751 with self-related immunity. *Genome Res.* 2014;24(10):1603-12.
752 61. Sood A, Lebel ME, Dong M, Fournier M, Vobecky SJ, Haddad E, et al. CD5 levels define
753 functionally heterogeneous populations of naive human CD4(+) T cells. *Eur J Immunol.*
754 2021;51(6):1365-76.
755 62. Hogquist KA, and Jameson SC. The self-obsession of T cells: how TCR signaling thresholds
756 affect fate 'decisions' and effector function. *Nat Immunol.* 2014;15(9):815-23.
757 63. Wadenpohl J, Seyfarth J, Hehenkamp P, Hoffmann M, Kummer S, Reinauer C, et al. CD5-
758 expressing CD8(+) T-cell subsets differ between children with type 1 diabetes and controls.
759 *Immunol Cell Biol.* 2021;99(10):1077-84.
760 64. Voisinne G, Gonzalez de Peredo A, and Roncagalli R. CD5, an Undercover Regulator of
761 TCR Signaling. *Front Immunol.* 2018;9:2900.
762 65. Lozano F, Simarro M, Calvo J, Vila JM, Padilla O, Bowen MA, et al. CD5 signal
763 transduction: positive or negative modulation of antigen receptor signaling. *Crit Rev*
764 *Immunol.* 2000;20(4):347-58.

765 66. Matson CA, Choi S, Livak F, Zhao B, Mitra A, Love PE, et al. CD5 dynamically calibrates
766 basal NF-kappaB signaling in T cells during thymic development and peripheral activation.
767 *Proc Natl Acad Sci U S A.* 2020;117(25):14342-53.
768 67. Axtell RC, Xu L, Barnum SR, and Raman C. CD5-CK2 binding/activation-deficient mice
769 are resistant to experimental autoimmune encephalomyelitis: protection is associated with
770 diminished populations of IL-17-expressing T cells in the central nervous system. *J Immunol.*
771 2006;177(12):8542-9.
772 68. Wong CP, Li L, Frelinger JA, and Tisch R. Early autoimmune destruction of islet grafts is
773 associated with a restricted repertoire of IGRP-specific CD8+ T cells in diabetic nonobese
774 diabetic mice. *J Immunol.* 2006;176(3):1637-44.
775 69. Hong X, Meng S, Tang D, Wang T, Ding L, Yu H, et al. Single-Cell RNA Sequencing
776 Reveals the Expansion of Cytotoxic CD4(+) T Lymphocytes and a Landscape of Immune
777 Cells in Primary Sjogren's Syndrome. *Front Immunol.* 2020;11:594658.
778 70. Rosati E, Pogorelyy MV, Dowds CM, Moller FT, Sorensen SB, Lebedev YB, et al.
779 Identification of Disease-associated Traits and Clonotypes in the T Cell Receptor Repertoire
780 of Monozygotic Twins Affected by Inflammatory Bowel Diseases. *J Crohns Colitis.*
781 2020;14(6):778-90.
782 71. Ihantola EL, Ilmonen H, Kailaanmaki A, Rytkonen-Nissinen M, Azam A, Maillere B, et al.
783 Characterization of Proinsulin T Cell Epitopes Restricted by Type 1 Diabetes-Associated
784 HLA Class II Molecules. *J Immunol.* 2020;204(9):2349-59.
785 72. Shizuru JA, Taylor-Edwards C, Livingstone A, and Fathman CG. Genetic dissection of T
786 cell receptor V beta gene requirements for spontaneous murine diabetes. *J Exp Med.*
787 1991;174(3):633-8.

788 73. Wucherpfennig KW, and Gagnon E. Positively selecting peptides: their job does not end in
789 the thymus. *Nat Immunol.* 2009;10(11):1143-4.
790 74. Daniels MA, Teixeiro E, Gill J, Hausmann B, Roubaty D, Holmberg K, et al. Thymic
791 selection threshold defined by compartmentalization of Ras/MAPK signalling. *Nature.*
792 2006;444(7120):724-9.
793 75. Rogers D, Sood A, Wang H, van Beek JJP, Rademaker TJ, Artusa P, et al. Pre-existing
794 chromatin accessibility and gene expression differences among naive CD4(+) T cells
795 influence effector potential. *Cell Rep.* 2021;37(9):110064.
796 76. Drobek A, Moudra A, Mueller D, Huranova M, Horkova V, Pribikova M, et al. Strong
797 homeostatic TCR signals induce formation of self-tolerant virtual memory CD8 T cells.
798 *EMBO J.* 2018;37(14).
799 77. Bolotin DA, Poslavsky S, Mitrophanov I, Shugay M, Mamedov IZ, Putintseva EV, et al.
800 MiXCR: software for comprehensive adaptive immunity profiling. *Nat Methods.*
801 2015;12(5):380-1.
802 78. Bagaev DV, Zvyagin IV, Putintseva EV, Izraelson M, Britanova OV, Chudakov DM, et al.
803 VDJviz: a versatile browser for immunogenomics data. *BMC Genomics.* 2016;17:453.
804 79. Kyte J, and Doolittle RF. A simple method for displaying the hydropathic character of a
805 protein. *J Mol Biol.* 1982;157(1):105-32.
806
807
808
809
810

Figures and figure legends

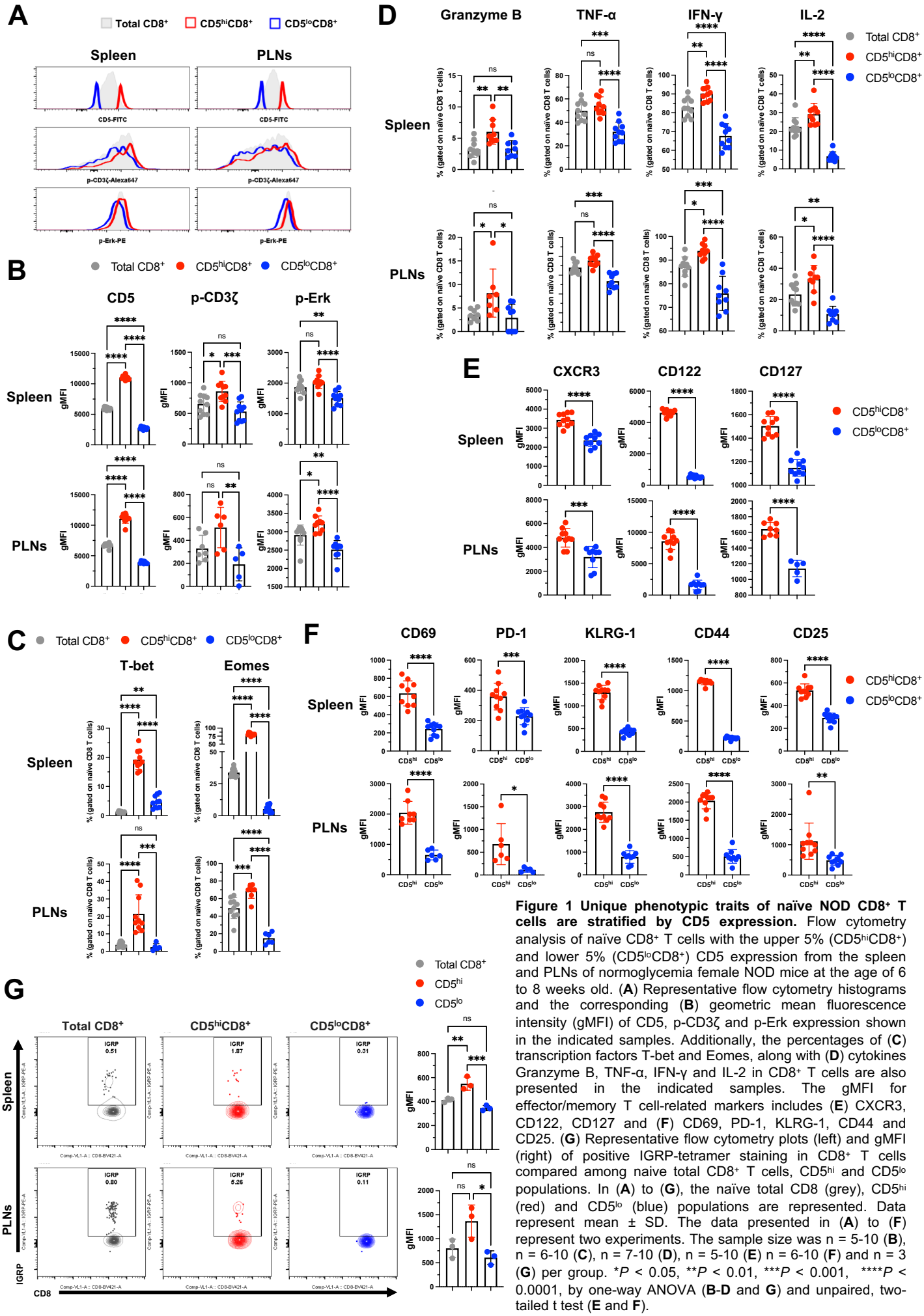

Figure 1 Unique phenotypic traits of naïve NOD CD8⁺ T cells are stratified by CD5 expression. Flow cytometry analysis of naïve CD8⁺ T cells with the upper 5% ($CD5^{hi}CD8^+$) and lower 5% ($CD5^{lo}CD8^+$) CD5 expression from the spleen and PLNs of normoglycemia female NOD mice at the age of 6 to 8 weeks old. (**A**) Representative flow cytometry histograms and the corresponding (**B**) geometric mean fluorescence intensity (gMFI) of CD5, p-CD3ζ and p-Erk expression shown in the indicated samples. Additionally, the percentages of (**C**) transcription factors T-bet and Eomes, along with (**D**) cytokines Granzyme B, TNF-α, IFN-γ and IL-2 in CD8⁺ T cells are also presented in the indicated samples. The gMFI for effector/memory T cell-related markers includes (**E**) CXCR3, CD122, CD127 and (**F**) CD69, PD-1, KLRG-1, CD44 and CD25. (**G**) Representative flow cytometry plots (left) and gMFI (right) of positive IGRP-tetramer staining in CD8⁺ T cells compared among naive total CD8⁺ T cells, $CD5^{hi}$ and $CD5^{lo}$ populations. In (**A**) to (**G**), the naïve total CD8 (grey), $CD5^{hi}$ (red) and $CD5^{lo}$ (blue) populations are represented. Data represent mean ± SD. The data presented in (**A**) to (**F**) represent two experiments. The sample size was n = 5-10 (**B**), n = 6-10 (**C**), n = 7-10 (**D**), n = 5-10 (**E**) n = 6-10 (**F**) and n = 3 (**G**) per group. *$P < 0.05$, **$P < 0.01$, ***$P < 0.001$, ****$P < 0.0001$, by one-way ANOVA (**B-D** and **G**) and unpaired, two-tailed t test (**E** and **F**).

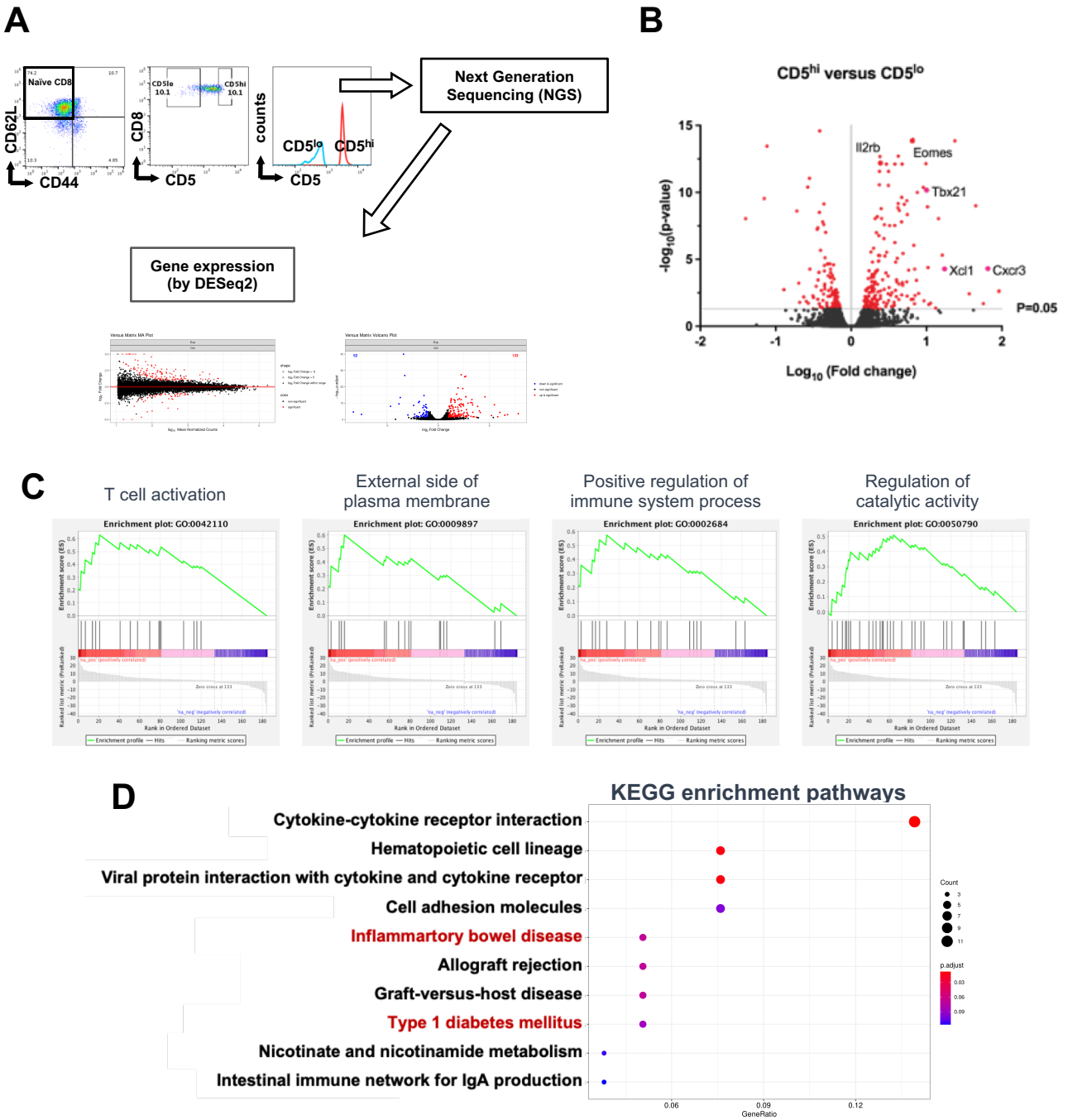

Figure 2 The gene expression profile of naïve CD5^{hi}CD8^{+} T cells reveals a poised phenotype for effector T cells in autoimmune diseases. (**A**) RNA-Seq performed on the sorted 10% upper and lower CD5-expressing of naïve CD8^{+} T cells (CD5^{hi}CD8^{+} and CD5^{lo}CD8^{+}) from 6-8-week-old normoglycemia female NOD mice to understand the gene expression profile of CD5^{hi}CD8^{+} T cells and comparing that to the CD5^{lo} counterpart to gain insights into their potential role in autoimmune diseases. (**B**) The volcano plot displaying the transcripts that are upregulated and downregulated by RNA sequencing of naïve CD5^{hi}CD8^{+} T cells compared to CD5^{lo}CD8^{+} T cells. The plot shows the log10 fold change of each transcript and the significance of the change, measured by the negative log10 of the adjusted *P*-value (adj.p). Genes with higher fold changes and lower adj.p values (red plots) indicate a significant change in expression between the two groups. (**C**) The gene set enrichment score plot for gene ontology terms (T cell activation, external side of plasma membrane, positive regulation of immune system process, and regulation of catalytic activity). Higher scores indicate a higher degree of enrichment of these processes in naïve CD5^{hi}CD8^{+} T cells compared to the CD5^{lo} counterpart. (**D**) The dot plots of the significant KEGG gene set enrichment in the top 10 enriched pathways, reinforcing the presence of a poised phenotype for effector T cells in autoimmune diseases in naïve CD5^{hi}CD8^{+} T cells. The data presented in (**A**) to (**D**) represent two experiments. In (**A**) to (**D**), n=10 mice per CD5^{hi}CD8^{+} or CD5^{lo}CD8^{+} group, with pooled spleen and PLN cells for sorting obtained from a total of 20 normoglycemia female NOD mice aged 6 to 8 weeks old. Significance is determined using a false discovery rate (FDR) adjusted *P*-value < 0.05 and validated using multiple testing correction method Benjamini-Hochberg correction.

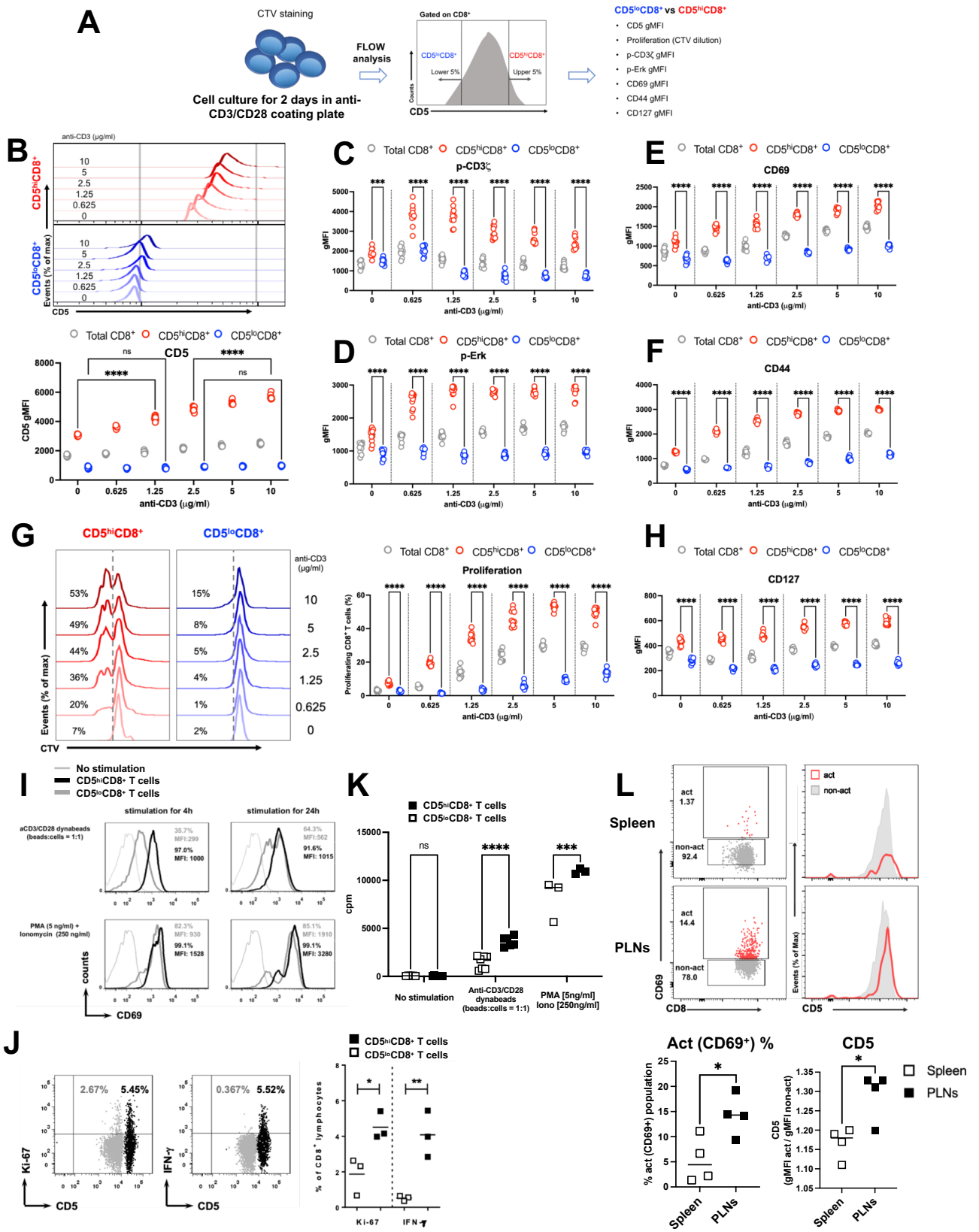

Figure 3 CD5 expression distinguishes CD8⁺ T cell subsets with differential activation and proliferation. (**A**) Diagram depicting naïve CD8⁺ T cells from normoglycemic female NOD mice aged 6 to 8 weeks, stimulated with indicated concentrations of anti-CD3 (0-10 μg/ml) and anti-CD28 (2 μg/ml; 0 μg/ml for control) for 2 days. Flow cytometry diagrams (**B** and **G**, upper and left panel, respectively) and statistical results (**B-H**) were derived from FLOW analysis. Comparison of CD5 (**B**), p-CD3ζ (**C**), p-Erk (**D**), CD69 (**E**), CD44 (**F**) expression, proliferation levels (CTV dilution percentage) (**G**), and CD127 expression (**H**) between 5% of upper (CD5^{hi}) and lower (CD5^{lo}) CD5-expressing CD8⁺ populations was conducted using gMFI of indicated markers. (**I**) Histogram comparing CD69 expression between the upper and lower 10% of CD5-expressing CD8⁺ T cells (CD5^{hi}CD8⁺ and CD5^{lo}CD8⁺). Naïve T cells from normoglycemic female NOD mice aged 6 to 8 weeks were stimulated with anti-CD3/CD28 dynabeads or PMA plus Ionomycin for specified durations and analyzed for CD69 expression by flow cytometry. (**J**) Comparison of Ki-67 expression and IFN-γ production by flow cytometry between CD5^{hi}CD8⁺ and CD5^{lo}CD8⁺ T cells isolated from normoglycemic female NOD mice aged 6 to 8 weeks. (**K**) Stimulation of CD5^{hi}CD8⁺ and CD5^{lo}CD8⁺ T cells isolated from normoglycemic female NOD mice aged 6 to 8 weeks with indicated amounts of anti-CD3/CD28 dynabeads or PMA plus Ionomycin for 2 days. Cell proliferation was assessed by [methyl-3H] thymidine incorporation (cpm; counts per minute). (**L**) Comparison of CD5 gMFI in CD8⁺CD69⁺ (upper gate of flow dot plot) to that in CD8⁺CD69⁻ (lower gate of flow dot plot) population by histogram (CD8⁺CD69⁺ in solid red line; CD8⁺CD69⁻ in grey), across spleen and PLNs from normoglycemic female NOD mice aged 6 to 8 weeks. The statistical results of the percentages of activated (CD8⁺CD69⁺) population (left) and the ratio of activated to non-activated CD5 gMFI (right) are shown. Data represent mean ± SD. The data presented in (**B**) to (**H**) represent two experiments. The sample size was n = 10 (**B-H**), n = 3 (**J**), n = 3-7 (**K**), and n = 4 (**L**) per group. *$P < 0.05$, **$P < 0.01$, ***$P < 0.001$, ****$P < 0.0001$, by two-way ANOVA (**B-K**) and unpaired, two-tailed t test (**L**).

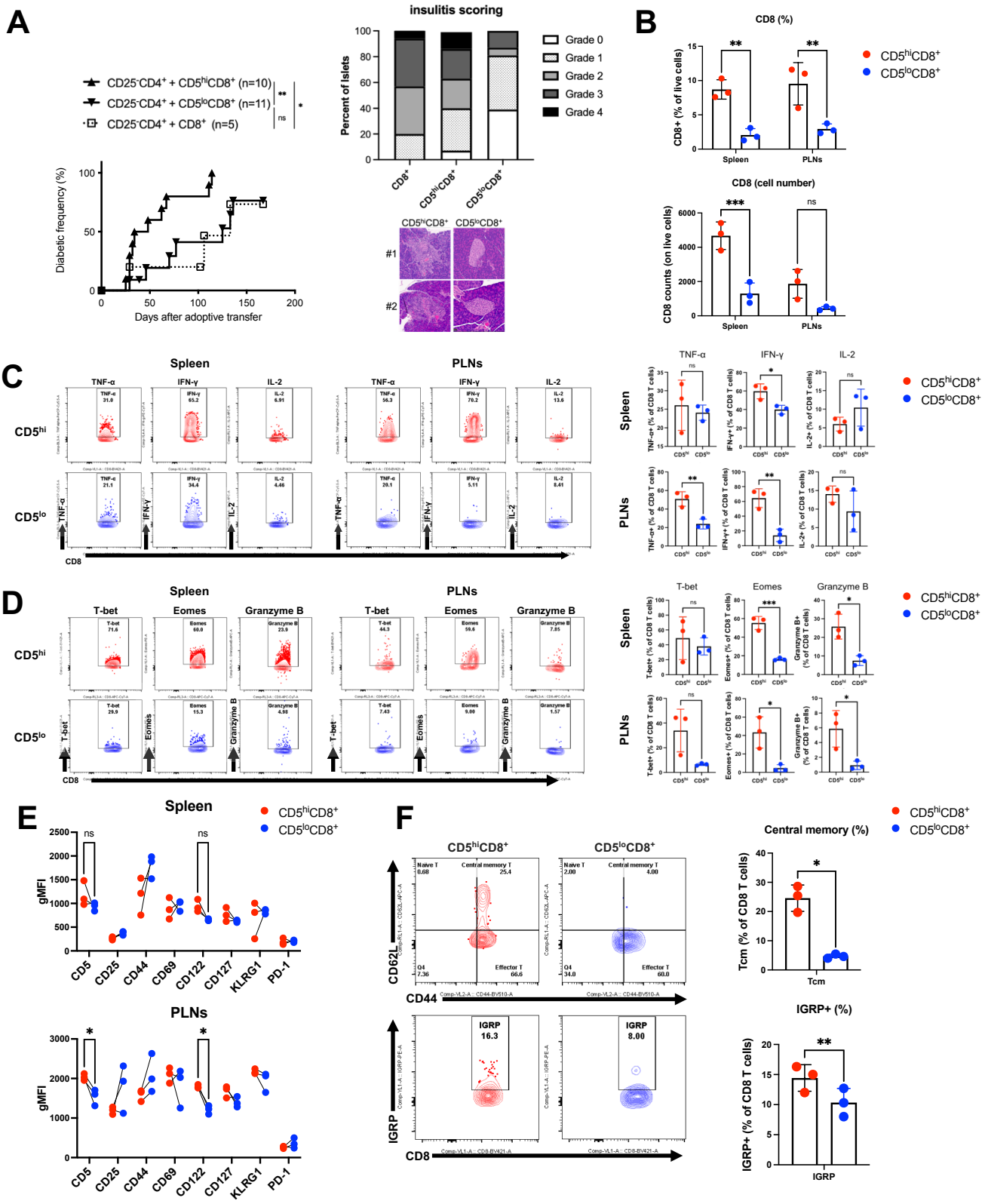

Figure 4 CD5^{hi}CD8^{+} T cells-transferred group exhibits severe insulitis and disease phenotype. (**A**) Diabetes incidence (left) in NOD Rag1$^{-/-}$ mice transferred with CD5^{hi}CD8^{+}, CD5^{lo}CD8^{+}, or CD8^{+} T cells, combined with CD4^{+} T cells, respectively. The islet histological analyses and insulitis scoring (right) for the mice after a 4-week transfer in the respective transferred groups showed a higher spontaneous diabetes frequency in the CD5^{hi}CD8^{+} group compared to the CD5^{lo}CD8^{+} group. The cells were sorted from the 10% upper and lower of CD5 expression of naïve CD8^{+} T cells (CD5^{hi}CD8^{+} and CD5^{lo}CD8^{+} T cells) from 6-8-week-old normoglycemic female NOD mice and adoptively transferred to 6-8-week-old female NOD Rag1$^{-/-}$ recipients via i.p. injection. Urine glucose concentrations of the four groups of mice were monitored weekly for spontaneous diabetes incidence. Diabetes was defined as glycosuria > 500 mg/dl in two consecutive tests. Insulitis scoring criteria can be found in the supplementary materials and methods. (**B**) Percentages and cell numbers of CD8^{+} T cells in spleen and PLNs, analyzed from CD5^{hi}CD8^{+} and CD5^{lo}CD8^{+} cells-transferred group, respectively, after 4-week adoptive transfer. (**C**) Percentages of TNF-α, IFN-γ and IL-2 production in CD5^{hi}CD8^{+} and CD5^{lo}CD8^{+} group, respectively, from spleen or PLNs, analyzed by flow cytometry, with representative flow dot plots (left) and statistical results (right). (**D**) Percentages of T-bet, Eomes and Granzyme B-expressing in CD5^{hi}CD8^{+} and CD5^{lo}CD8^{+} group, respectively, from spleen or PLNs, analyzed by flow cytometry, with representative flow dot plots (left) and statistical results (right). (**E**) Comparison of differential gMFI expression of CD5, CD25, CD44, CD69, CD122, CD127, KLRG1 and PD-1 between CD5^{hi}CD8^{+} and CD5^{lo}CD8^{+} group from spleen or PLNs. (**F**) Comparison of percentages of central memory T cells (defined by CD44^{hi}CD62L^{hi}) (upper) and positive IGRP-tetramer staining (lower) between CD5^{hi}CD8^{+} and CD5^{lo}CD8^{+} groups from PLNs, with representative flow dot plots (left) and statistical results (right). Data represent mean ± SD. Sample size was n = 5-11 (**A**), and n = 3 (**B-F**) per group. *P < 0.05, **P < 0.01, ***P < 0.001, by log-rank test (**A**), by two-way ANOVA (**B**) and (**E**) and unpaired, two-tailed t test (**C**), (**D**) and (**F**).

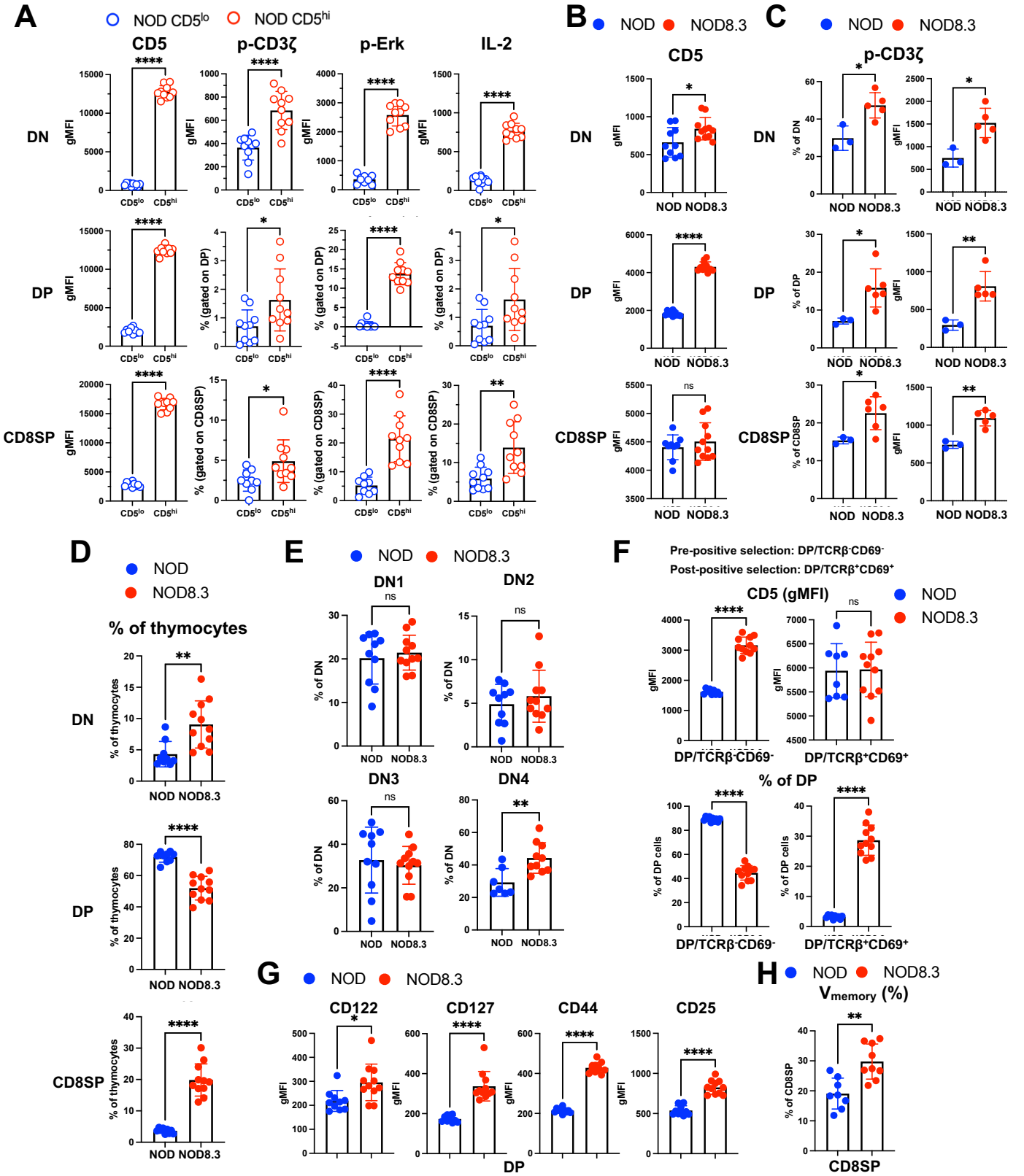

Figure 5 The high CD5-linked TCR basal signals positively correlate with thymic selection in autoimmune-poised NOD8.3 mice. (**A**) CD5, p-CD3ζ, p-Erk and IL-2 expression levels compared between the lower 5% (hollow blue) and upper 5% (hollow red) CD5 expression in thymocytes of normoglycemia female NOD mice aged 6 to 8 weeks old across DN, DP and CD8SP stages. (**B-H**) Comparison of various marker expression levels between thymocytes of normoglycemia female NOD (solid blue) and NOD8.3 (solid red) mice aged 6 to 8 weeks old across different selection stages. (**B**) CD5 gMFI in NOD and NOD8.3 thymocytes across DN, DP and CD8SP stages. (**C**) Percentages of p-CD3ζ (left) and the corresponding gMFI of p-CD3 (right) compared between NOD and NOD8.3 thymocytes in the indicated stages DN, DP and CD8SP. (**D**) Percentages of DN, DP and CD8SP composition compared between NOD and NOD8.3 thymocytes. (**E**) Percentages of indicated DN stages (DN1, DN2, DN3 and DN4) in the DN subset compared between NOD and NOD8.3 mice. DN stages are defined as follows: DN1 ($CD44^+CD25^-$), DN2 ($CD44^+CD25^+$), DN3 ($CD44^-CD25^+$) and DN4 ($CD44^-CD25^-$), as depicted in the gating shown in Supplementary Figure 3A, middle panels. (**F**) CD5 gMFI (upper) and corresponding percentages (lower) in the pre-positive selection ($TCR\beta^-CD69^-$) and post-positive selection ($TCR\beta^+CD69^+$) populations in DP thymocytes compared between NOD and NOD8.3 mice. The presence of higher TCR basal signals (indicated by higher CD5 gMFI) in NOD8.3 in the pre-positive selection stage leads to an increased percentage of $TCR\beta^+CD69^+$ cells in the post-selection stage compared to NOD mice, as shown in Supplementary Figure 3F. (**G**) gMFI of CD122, CD127, CD44 and CD25 assessed in DP thymocytes compared between NOD and NOD8.3 mice. (**H**) Percentages of virtual memory (V_{memory}) cells in CD8SP thymocytes compared between NOD and NOD8.3 mice. Data represent mean ± SD. The data presented in (**B**) to (**H**) represent two experiments. The sample size was n = 10 (**A**), n = 10-11 (**B**), n = 3-6 (**C**), n = 9-11 (**D**), n = 7-11 (**E**), n = 8-11 (**F**) n = 10-11 (**G**) and n = 8-9 (**H**) per group. *$P < 0.05$, **$P < 0.01$, ****$P < 0.0001$, by unpaired, two-tailed t test (**A-H**).

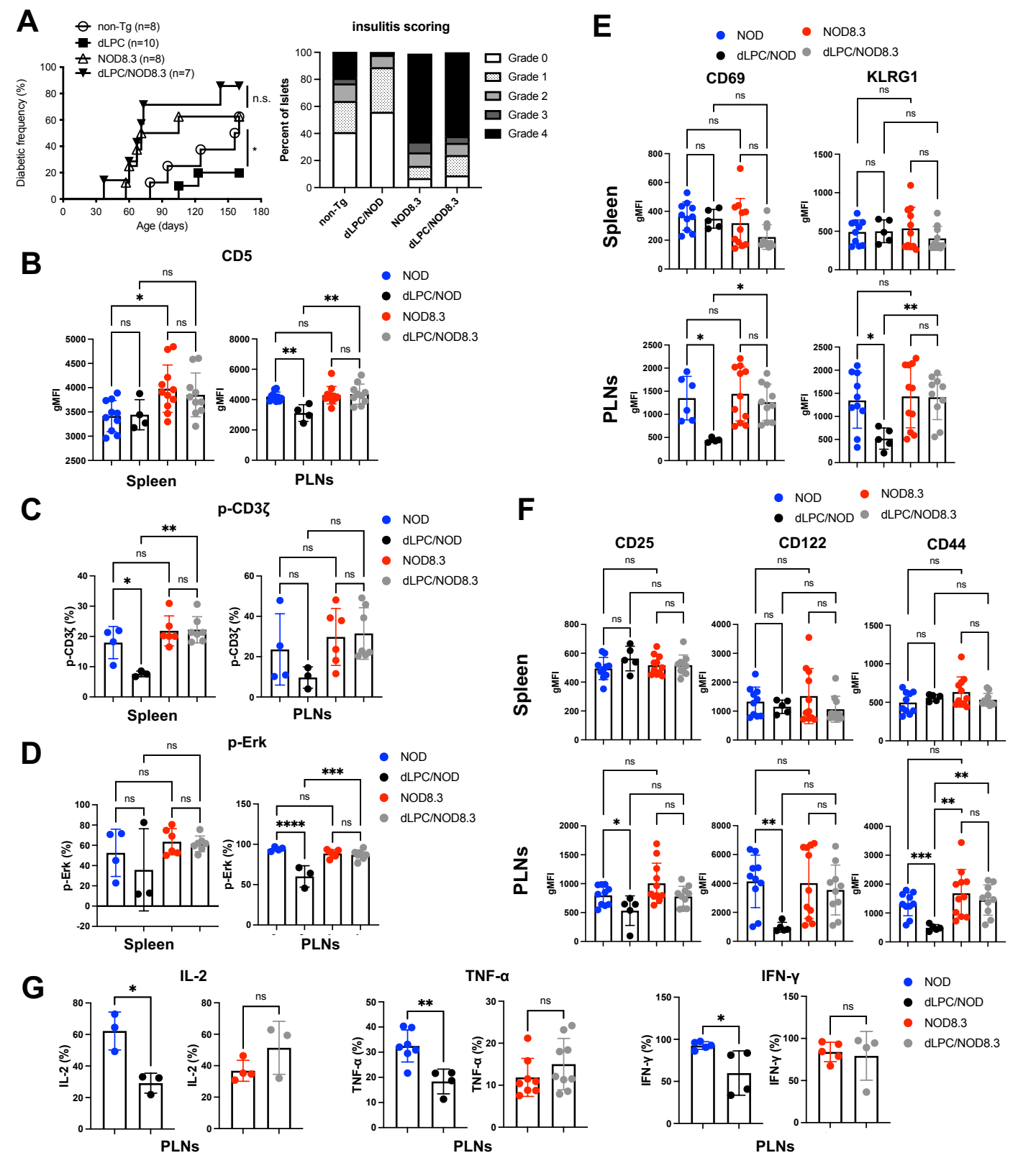

Figure 6 The protective effect of transgenic Pep on diabetogenesis is negated in dLPC/NOD8.3 mice. (**A**) Spontaneous diabetes incidence (left) and insulitis scoring (right) of female non-Tg NOD, dLPC/NOD, NOD8.3 and dLPC/NOD8.3 mice. Insulitis scoring was performed on the islets from the pancreata of 6-8-week-old mice before the onset of diabetes in each group. Insulitis scoring criteria can be found in the supplementary materials and methods. Urine glucose concentrations of mice were monitored weekly for spontaneous diabetes incidence. Diabetes was defined as glycosuria > 500 mg/dl at two consecutive tests. (**B**-**G**) Characterization of various aspects of TCR signal strength and effector/memory T cell phenotypes among female normoglycemia non-Tg NOD (blue), dLPC/NOD (black), NOD8.3 (red) and dLPC/NOD8.3 (grey) mice at the age of 6 to 8 weeks old. (**B**) CD5 gMFI of $CD8^+$ T cells in the spleen (left) and PLNs (right). (**C**) Percentage of p-$CD3\zeta^+CD8^+$ T cells in the spleen (left) and PLNs (right). (**D**) Percentage of p-Erk^+CD8^+ T cells in the spleen (left) and PLNs (right). (**E**) gMFI of effector T cell markers CD69 and KLRG1 in $CD8^+$ T cells from the spleen (upper) and PLNs (lower). (**F**) gMFI of memory T cell markers CD25, CD122 and CD44 in $CD8^+$ T cells from the spleen (upper) and PLNs (lower). (**G**) Percentage of IL-2^+-, TNF-α^+-, and IFN-γ^+CD8^+ T cells in PLNs. Data in (**B**) to (**G**) represent mean ± SD. The data presented in (**B**) to (**G**) represent two experiments. The sample size was n = 7-10 (**A**), n = 4-11 (**B**), n = 3-7 (**C**), n = 3-7 (**D**), n = 5-11 (**E**), n = 5-11 (**F**) and n = 3-9 (**G**) per group. *$P < 0.05$, **$P < 0.01$, ***$P < 0.001$, ****$P < 0.0001$, by log-rank test (**A**), by one-way ANOVA (**B**-**F**) and unpaired, two-tailed t test (**G**).

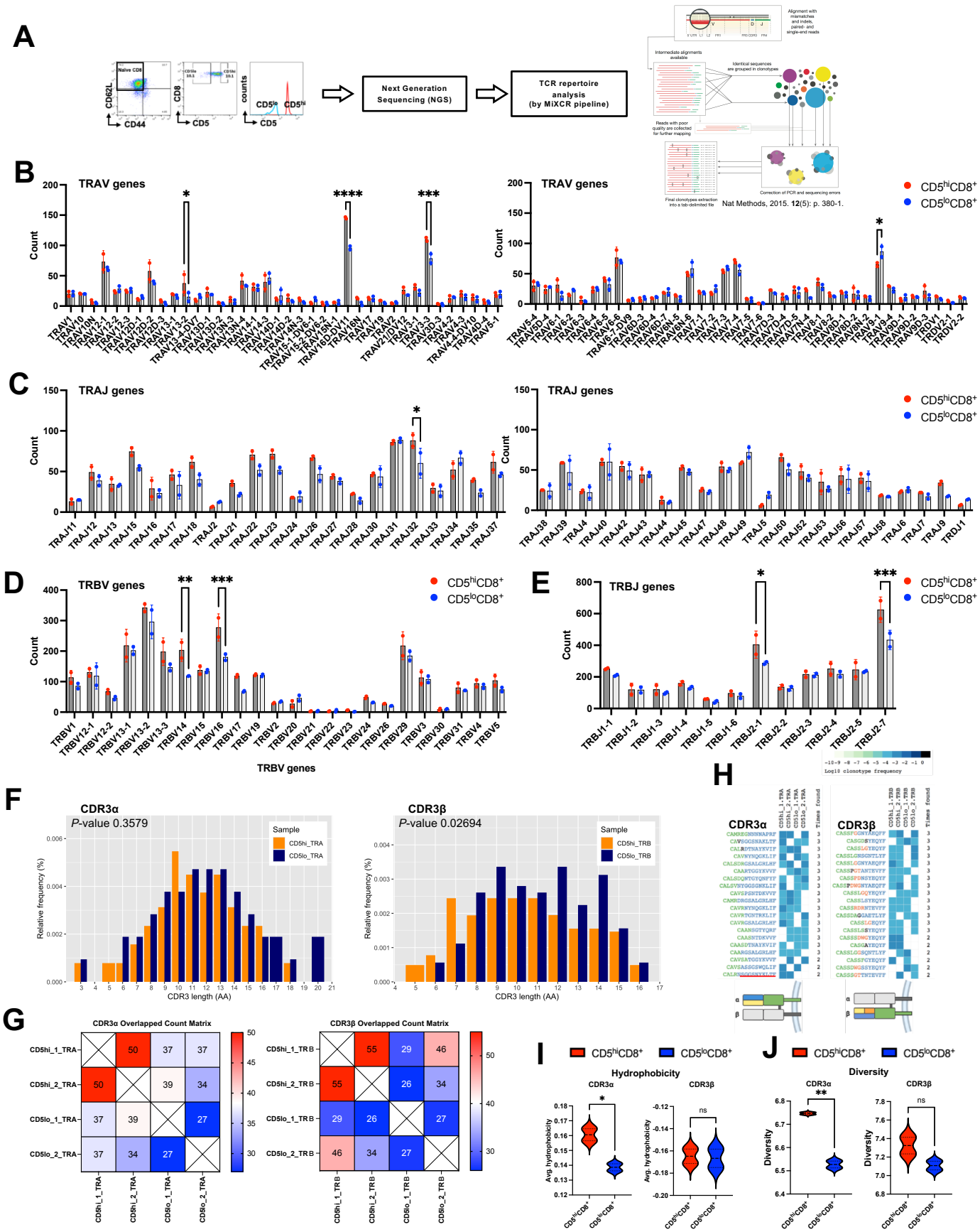

Figure 7 Examination of the CD5^{hi} population reveals TCR repertoires linked to autoimmune disorders. (**A**) Comparison of TCR repertoire differences between CD5^{hi}CD8$^+$ and CD5^{lo}CD8$^+$ T cell populations conducted using bulk RNA sequencing, followed by TCR repertoire analysis using the MiXCR pipeline. Naïve CD5^{hi}CD8$^+$ and CD5^{lo}CD8$^+$ cells were sorted from female normoglycemia NOD mice aged 6 to 8 weeks old following a similar procedure as outlined in Figure 2A, with 1.5 x 10^6 cells per group. The TCR repertoire of naïve CD5^{hi}CD8$^+$ T cells exhibited shorter CDR3 lengths, higher clone overlap values within group comparisons, pathogenic-related CDR3 motifs, and greater hydrophobicity and diversity in the TRA chain compared to CD8$^+$CD5^{lo} cells. (**B-E**) Comparison of the TRAV gene segment usage (**B**), TRAJ gene segment usage (**C**), TRBV gene segment usage (**D**), and TRBJ gene segment usage (**E**) within TRA variable and TRB variable genes between CD5^{hi}CD8$^+$ (red) and CD5^{lo}CD8$^+$ (blue) cells. (**F-J**) Comparison of CDR3α (left) or CDR3β (right) length in amino acids (**F**), CDR3 clonal overlap by overlapped count matrix (**G**), top 20 CDR3 motifs (**H**), average hydrophobicity score (**I**) and diversity (**J**) of CDR3α (left) and CDR3β (right) between CD5^{hi}CD8$^+$ and CD5^{lo}CD8$^+$ T cells. In (**G**), number in cell indicates count number shared within the comparison group. (**H**) Occurrence frequencies of the top 20 CDR3 motifs from mapped-CDR3α (left) and CDR3β (right) sequencings in CD5^{hi}CD8$^+$ and CD5^{lo}CD8$^+$ cells, with the high-occurrence rate of the CDR3α motif "SGGSNYKLTF" (underlined in red) specific to T1D-related IGRP peptide in the CD8$^+$CD5^{hi} population. (**I**) Average hydrophobicity score defined by summing up the hydrophobicity score in each amino acid in the CDR3 motif and dividing by the CDR3 length, then averaging by total counts in each group. Diversity definition in (**J**) is shown in Materials and Methods section Clonotype repertoire metrics formulas. In (**B-E**), each point represents 10 mice, with two points for each group, totaling n = 20 mice (**F-J**) for all CD5^{hi} or CD5^{lo} samples. *P < 0.05, **P < 0.01, ***P < 0.001, by two-way ANOVA (**B-E**), by Welch two sample t-test (**F**), and unpaired, two-tailed t test (**I**) and (**J**).

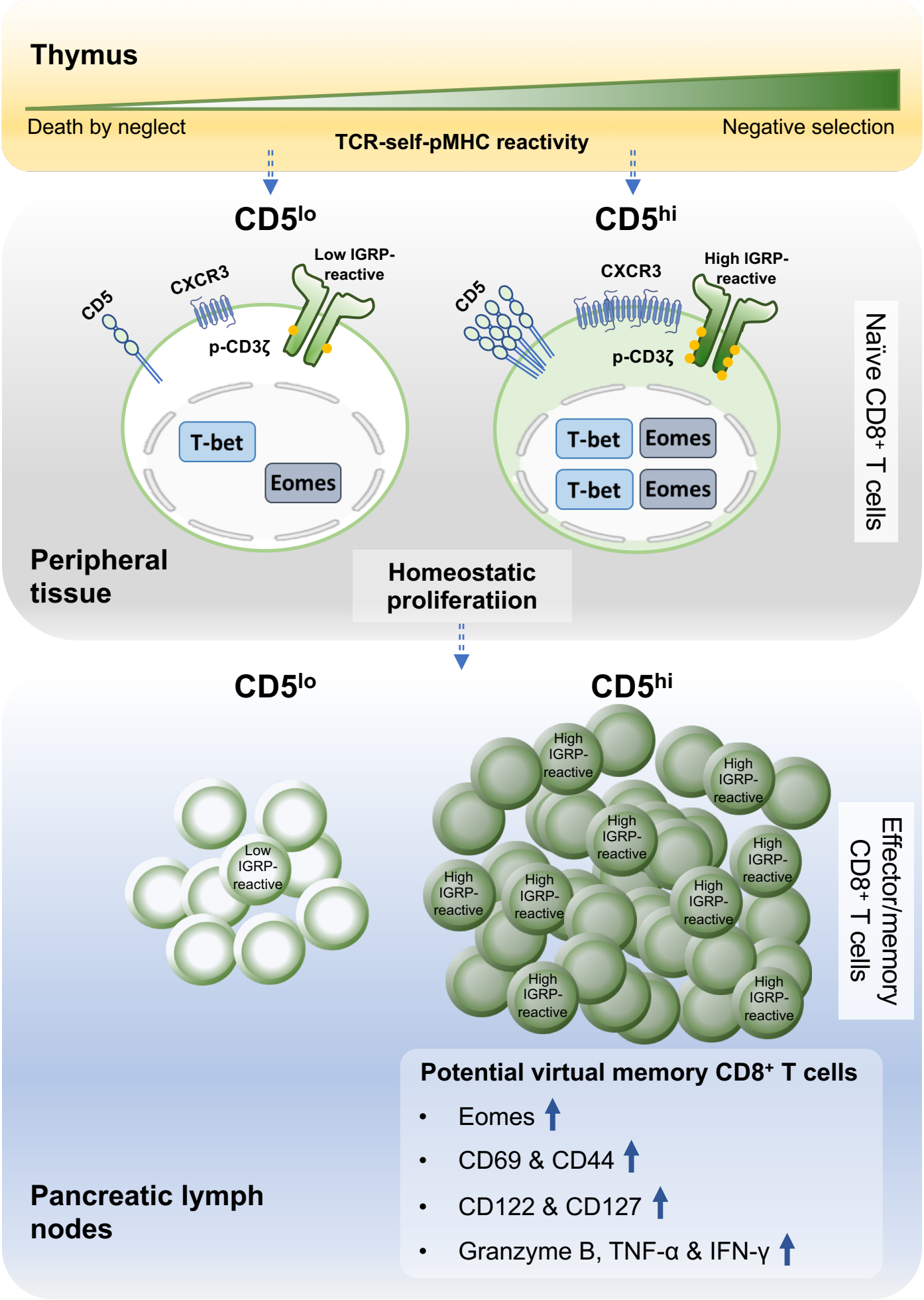

Figure 8 Thymocyte self-reactivity impacts the effector functions and memory cell formation of auto-reactive T cells in the T1D model NOD mice.

Table

Table 1 Naïve $CD5^{hi}CD8^{+}$ and $CD5^{lo}CD8^{+}$ T cells exhibit distinct expression in effector/memory T cell gene-expression clusters.

Cluster	Characteristics	$CD5^{lo}$	$CD5^{hi}$	*P*	Proportion
I	Initial cytokine or effector response	2	21	6.66555E-45	0.913
II	Preparation for cell division	98	406	1.7815E-173	0.806
III	Cell cycle & division	81	175	2.20063E-29	0.684
IV	Naive and late memory	44	25	5.78321E-06	0.362
V	Early effector, late memory	33	150	2.31501E-70	0.820
VI	Short-term effector and memory	18	30	0.000881688	0.625
VII	Memory precursor	47	41	0.251118001	0.466
VIII	Naive or late effector or memory	103	98	0.492702408	0.488
IX	Short-term effector or memory	27	45	6.4806E-05	0.625
X	Late effector or memory	28	49	1.77113E-06	0.636

Variation in gene-expression clusters between naïve $CD5^{hi}CD8^{+}$ and $CD5^{lo}CD8^{+}$ T cells and gene-set clusters in $CD8^{+}$ T cells evaluated by the Immunological Genome Project (published clusters with designated characteristics). In the '$CD5^{lo}$' and '$CD5^{hi}$' columns, values represent the count of genes predominantly expressed in each subset; 'Proportion' indicates the fraction of those genes expressed in the $CD5^{hi}$ subset. Statistical significance of expression differences was determined using the $\chi 2$ test (*P*).

811 ## Figure legends

812 **Figure 1 Unique phenotypic traits of naïve NOD CD8$^+$ T cells are stratified by CD5**
813 **expression.** Flow cytometry analysis of naïve CD8$^+$ T cells with the upper 5% (CD5^{hi}CD8$^+$) and
814 lower 5% (CD5^{lo}CD8$^+$) CD5 expression from the spleen and PLNs of normoglycemia female NOD
815 mice at the age of 6 to 8 weeks old. (**A**) Representative flow cytometry histograms and the
816 corresponding (**B**) geometric mean fluorescence intensity (gMFI) of CD5, p-CD3ζ and p-Erk
817 expression shown in the indicated samples. Additionally, the percentages of (**C**) transcription
818 factors T-bet and Eomes, along with (**D**) cytokines Granzyme B, TNF-α, IFN-γ and IL-2 in CD8$^+$
819 T cells are also presented in the indicated samples. The gMFI for effector/memory T cell-related
820 markers includes (**E**) CXCR3, CD122, CD127 and (**F**) CD69, PD-1, KLRG-1, CD44 and CD25.
821 (**G**) Representative flow cytometry plots (left) and gMFI (right) of positive IGRP-tetramer staining
822 in CD8$^+$ T cells compared among naive total CD8$^+$ T cells, CD5^{hi} and CD5^{lo} populations. In (**A**)
823 to (**G**), the naïve total CD8 (grey), CD5^{hi} (red) and CD5^{lo} (blue) populations are represented. Data
824 represent mean ± SD. The data presented in (**A**) to (**F**) represent two experiments. The sample size
825 was n = 5-10 (**B**), n = 6-10 (**C**), n = 7-10 (**D**), n = 5-10 (**E**) n = 6-10 (**F**) and n = 3 (**G**) per group.
826 *$P < 0.05$, **$P < 0.01$, ***$P < 0.001$, ****$P < 0.0001$, by one-way ANOVA (**B-D** and **G**) and
827 unpaired, two-tailed t test (**E** and **F**).

828

829 **Figure 2 The gene expression profile of naïve CD5^{hi}CD8$^+$ T cells reveals a poised phenotype**
830 **for effector T cells in autoimmune diseases.** (**A**) RNA-Seq performed on the sorted 10% upper
831 and lower CD5-expressing of naïve CD8$^+$ T cells (CD5^{hi}CD8$^+$ and CD5^{lo}CD8$^+$) from 6-8-week-
832 old normoglycemia female NOD mice to understand the gene expression profile of CD5^{hi}CD8$^+$ T
833 cells and comparing that to the CD5^{lo} counterpart to gain insights into their potential role in

834 autoimmune diseases. (**B**) The volcano plot displaying the transcripts that are upregulated and
835 downregulated by RNA sequencing of naïve $CD5^{hi}CD8^{+}$ T cells compared to $CD5^{lo}CD8^{+}$ T cells.
836 The plot shows the log10 fold change of each transcript and the significance of the change,
837 measured by the negative log10 of the adjusted *P*-value (adj.p). Genes with higher fold changes
838 and lower adj.p values (red plots) indicate a significant change in expression between the two
839 groups. (**C**) The gene set enrichment score plot for gene ontology terms (T cell activation, external
840 side of plasma membrane, positive regulation of immune system process, and regulation of
841 catalytic activity). Higher scores indicate a higher degree of enrichment of these processes in naïve
842 $CD5^{hi}CD8^{+}$ T cells compared to the $CD5^{lo}$ counterpart. (**D**) The dot plots of the significant KEGG
843 gene set enrichment in the top 10 enriched pathways, reinforcing the presence of a poised
844 phenotype for effector T cells in autoimmune diseases in naïve $CD5^{hi}CD8^{+}$ T cells. The data
845 presented in (**A**) to (**D**) represent two experiments. In (**A**) to (**D**), n=10 mice per $CD5^{hi}CD8^{+}$ or
846 $CD5^{lo}CD8^{+}$ group, with pooled spleen and PLN cells for sorting obtained from a total of 20
847 normoglycemia female NOD mice aged 6 to 8 weeks old. Significance is determined using a false
848 discovery rate (FDR) adjusted *P*-value < 0.05 and validated using multiple testing correction
849 method Benjamini-Hochberg correction.
850
851 **Figure 3 CD5 expression distinguishes $CD8^{+}$ T cell subsets with differential activation and**
852 **proliferation.** (**A**) Diagram depicting naïve $CD8^{+}$ T cells from normoglycemic female NOD mice
853 aged 6 to 8 weeks, stimulated with indicated concentrations of anti-CD3 (0-10 μg/ml) and anti-
854 CD28 (2 μg/ml; 0 μg/ml for control) for 2 days. Flow cytometry diagrams (**B** and **G**, upper and
855 left panel, respectively) and statistical results (**B-H**) were derived from FLOW analysis.
856 Comparison of CD5 (**B**), p-CD3ζ (**C**), p-Erk (**D**), CD69 (**E**), CD44 (**F**) expression, proliferation

857 levels (CTV dilution percentage) (**G**), and CD127 expression (**H**) between 5% of upper ($CD5^{hi}$)
858 and lower ($CD5^{lo}$) CD5-expressing $CD8^+$ populations was conducted using gMFI of indicated
859 markers. (**I**) Histogram comparing CD69 expression between the upper and lower 10% of CD5-
860 expressing $CD8^+$ T cells ($CD5^{hi}CD8^+$ and $CD5^{lo}CD8^+$). Naïve T cells from normoglycemic female
861 NOD mice aged 6 to 8 weeks were stimulated with anti-CD3/CD28 dynabeads or PMA plus
862 Ionomycin for specified durations and analyzed for CD69 expression by flow cytometry. (**J**)
863 Comparison of Ki-67 expression and IFN-γ production by flow cytometry between $CD5^{hi}CD8^+$
864 and $CD5^{lo}CD8^+$ T cells isolated from normoglycemic female NOD mice aged 6 to 8 weeks. (**K**)
865 Stimulation of $CD5^{hi}CD8^+$ and $CD5^{lo}CD8^+$ T cells isolated from normoglycemic female NOD
866 mice aged 6 to 8 weeks with indicated amounts of anti-CD3/CD28 dynabeads or PMA plus
867 Ionomycin for 2 days. Cell proliferation was assessed by [methyl-3H] thymidine incorporation
868 (cpm; counts per minute). (**L**) Comparison of CD5 gMFI in $CD8^+CD69^+$ (upper gate of flow dot
869 plot) to that in $CD8^+CD69^-$ (lower gate of flow dot plot) population by histogram ($CD8^+CD69^+$ in
870 solid red line; $CD8^+CD69^-$ in grey), across spleen and PLNs from normoglycemic female NOD
871 mice aged 6 to 8 weeks. The statistical results of the percentages of activated ($CD8^+CD69^+$)
872 population (left) and the ratio of activated to non-activated CD5 gMFI (right) are shown. Data
873 represent mean ± SD. The data presented in (**B**) to (**H**) represent two experiments. The sample size
874 was n = 10 (**B**-**H**), n = 3 (**J**), n = 3-7 (**K**), and n = 4 (**L**) per group. *$P < 0.05$, **$P < 0.01$, ***$P <$
875 0.001, ****$P < 0.0001$, by two-way ANOVA (**B**-**K**) and unpaired, two-tailed t test (**L**).
876
877 **Figure 4 $CD5^{hi}CD8^+$ T cells-transferred group exhibits severe insulitis and disease phenotype.**
878 (**A**) Diabetes incidence (left) in NOD $Rag1^{-/-}$ mice transferred with $CD5^{hi}CD8^+$, $CD5^{lo}CD8^+$, or
879 $CD8^+$ T cells, combined with $CD4^+$ T cells, respectively. The islet histological analyses and

880 insulitis scoring (right) for the mice after a 4-week transfer in the respective transferred groups
881 showed a higher diabetes frequency in the $CD5^{hi}CD8^{+}$ group compared to the $CD5^{lo}CD8^{+}$ group.
882 The cells were sorted from the 10% upper and lower of CD5 expression of naïve $CD8^{+}$ T cells
883 ($CD5^{hi}CD8^{+}$ and $CD5^{lo}CD8^{+}$ T cells) from 6-8-week-old normoglycemic female NOD mice and
884 adoptively transferred to 6-8-week-old female NOD $Rag1^{-/-}$ recipients via i.p. injection. Urine
885 glucose concentrations of the four groups of mice were monitored weekly for diabetes incidence.
886 Diabetes was defined as glycosuria > 500 mg/dl in two consecutive tests. Insulitis scoring criteria
887 can be found in the supplementary materials and methods. (**B**) Percentages and cell numbers of
888 $CD8^{+}$ T cells in spleen and PLNs, analyzed from $CD5^{hi}CD8^{+}$ and $CD5^{lo}CD8^{+}$ cells-transferred
889 group, respectively, after 4-week adoptive transfer. (**C**) Percentages of TNF-α, IFN-γ and IL-2
890 production in $CD5^{hi}CD8^{+}$ and $CD5^{lo}CD8^{+}$ group, respectively, from spleen or PLNs, analyzed by
891 flow cytometry, with representative flow dot plots (left) and statistical results (right). (**D**)
892 Percentages of T-bet, Eomes and Granzyme B-expressing in $CD5^{hi}CD8^{+}$ and $CD5^{lo}CD8^{+}$ group,
893 respectively, from spleen or PLNs, analyzed by flow cytometry, with representative flow dot plots
894 (left) and statistical results (right). (**E**) Comparison of differential gMFI expression of CD5, CD25,
895 CD44, CD69, CD122, CD127, KLRG1 and PD-1 between $CD5^{hi}CD8^{+}$ and $CD5^{lo}CD8^{+}$ group from
896 spleen or PLNs. (**F**) Comparison of percentages of central memory T cells (defined by
897 $CD44^{hi}CD62L^{hi}$) (upper) and positive IGRP-tetramer staining (lower) between $CD5^{hi}CD8^{+}$ and
898 $CD5^{lo}CD8^{+}$ groups from PLNs, with representative flow dot plots (left) and statistical results
899 (right). Data represent mean ± SD. Sample size was n = 5-11 (**A**), and n = 3 (**B**-**F**) per group. *P
900 < 0.05, **P < 0.01, ***P < 0.001, by log-rank test (**A**), by two-way ANOVA (**B**) and (**E**) and
901 unpaired, two-tailed t test (**C**), (**D**) and (**F**).

902 **Figure 5 The high CD5-linked TCR basal signals positively correlate with thymic selection**

903 **in autoimmune-poised NOD8.3 mice.** (**A**) CD5, p-CD3ζ, p-Erk and IL-2 expression levels
904 compared between the lower 5% (hollow blue) and upper 5% (hollow red) CD5 expression in
905 thymocytes of normoglycemia female NOD mice aged 6 to 8 weeks old across DN, DP and CD8SP
906 stages. (**B-H**) Comparison of various marker expression levels between thymocytes of
907 normoglycemia female NOD (solid blue) and NOD8.3 (solid red) mice aged 6 to 8 weeks old
908 across different selection stages. (**B**) CD5 gMFI in NOD and NOD8.3 thymocytes across DN, DP
909 and CD8SP stages. (**C**) Percentages of p-CD3ζ (left) and the corresponding gMFI of p-CD3 (right)
910 compared between NOD and NOD8.3 thymocytes in the indicated stages DN, DP and CD8SP. (**D**)
911 Percentages of DN, DP and CD8SP composition compared between NOD and NOD8.3
912 thymocytes. (**E**) Percentages of indicated DN stages (DN1, DN2, DN3 and DN4) in the DN subset
913 compared between NOD and NOD8.3 mice. DN stages are defined as follows: DN1
914 ($CD44^+CD25^-$), DN2 ($CD44^+CD25^+$), DN3 ($CD44^-CD25^+$) and DN4 ($CD44^-CD25^-$), as depicted
915 in the gating shown in Supplementary Figure 3A, middle panels. (**F**) CD5 gMFI (upper) and
916 corresponding percentages (lower) in the pre-positive selection ($TCR\beta^-CD69^-$) and post-positive
917 selection ($TCR\beta^+CD69^+$) populations in DP thymocytes compared between NOD and NOD8.3
918 mice. The presence of higher TCR basal signals (indicated by higher CD5 gMFI) in NOD8.3 in
919 the pre-positive selection stage leads to an increased percentage of $TCR\beta^+CD69^+$ cells in the post-
920 selection stage compared to NOD mice, as shown in Supplementary Figure 3F. (**G**) gMFI of
921 CD122, CD127, CD44 and CD25 assessed in DP thymocytes compared between NOD and
922 NOD8.3 mice. (**H**) Percentages of virtual memory (V_{memory}) cells in CD8SP thymocytes compared
923 between NOD and NOD8.3 mice. Data represent mean ± SD. The data presented in (**B**) to (**H**)
924 represent two experiments. The sample size was n = 10 (**A**), n = 10-11 (**B**), n = 3-6 (**C**), n = 9-11
925 (**D**), n = 7-11 (**E**), n = 8-11 (**F**) n = 10-11 (**G**) and n = 8-9 (**H**) per group. *$P < 0.05$, **$P < 0.01$,

926 ****$P < 0.0001$, by unpaired, two-tailed t test (**A-H**).

927

928 **Figure 6 The protective effect of transgenic Pep on diabetogenesis is negated in**
929 **dLPC/NOD8.3 mice.** (**A**) Spontaneous diabetes incidence (left) and insulitis scoring (right) of
930 female non-Tg NOD, dLPC/NOD, NOD8.3 and dLPC/NOD8.3 mice. Insulitis scoring was
931 performed on the islets from the pancreata of 6-8-week-old mice before the onset of diabetes in
932 each group. Insulitis scoring criteria can be found in the supplementary materials and methods.
933 Urine glucose concentrations of mice were monitored weekly for spontaneous diabetes incidence.
934 Diabetes was defined as glycosuria > 500 mg/dl at two consecutive tests. (**B-G**) Characterization
935 of various aspects of TCR signal strength and effector/memory T cell phenotypes among female
936 normoglycemia non-Tg NOD (blue), dLPC/NOD (black), NOD8.3 (red) and dLPC/NOD8.3 (grey)
937 mice at the age of 6 to 8 weeks old. (**B**) CD5 gMFI of $CD8^+$ T cells in the spleen (left) and PLNs
938 (right). (**C**) Percentage of p-$CD3\zeta^+CD8^+$ T cells in the spleen (left) and PLNs (right). (**D**)
939 Percentage of p-Erk^+CD8^+ T cells in the spleen (left) and PLNs (right). (**E**) gMFI of effector T cell
940 markers CD69 and KLRG1 in $CD8^+$ T cells from the spleen (upper) and PLNs (lower). (**F**) gMFI
941 of memory T cell markers CD25, CD122 and CD44 in $CD8^+$ T cells from the spleen (upper) and
942 PLNs (lower). (**G**) Percentage of IL-2^+-, TNF-α^+-, and IFN-γ^+CD8^+ T cells in PLNs. Data in (**B**)
943 to (**G**) represent mean ± SD. The data presented in (**B**) to (**G**) represent two experiments. The
944 sample size was n = 7-10 (**A**), n = 4-11 (**B**), n = 3-7 (**C**), n = 3-7 (**D**), n = 5-11 (**E**), n = 5-11 (**F**)
945 and n = 3-9 (**G**) per group. *$P < 0.05$, **$P < 0.01$, ***$P < 0.001$, ****$P < 0.0001$, by log-rank
946 test (**A**), by one-way ANOVA (**B-F**) and unpaired, two-tailed t test (**G**).

947

948 **Figure 7 Examination of the $CD5^{hi}$ population reveals TCR repertoires linked to**

949 **autoimmune disorders.** (**A**) Comparison of TCR repertoire differences between $CD5^{hi}CD8^{+}$ and
950 $CD5^{lo}CD8^{+}$ T cell populations conducted using bulk RNA sequencing, followed by TCR repertoire
951 analysis using the MiXCR pipeline. Naïve $CD5^{hi}CD8^{+}$ and $CD5^{lo}CD8^{+}$ cells were sorted from
952 female normoglycemia NOD mice aged 6 to 8 weeks old following a similar procedure as outlined
953 in Figure 2A, with 1.5 x 10^{6} cells per group. The TCR repertoire of naïve $CD5^{hi}CD8^{+}$ T cells
954 exhibited shorter CDR3 lengths, higher clone overlap values within group comparisons,
955 pathogenic-related CDR3 motifs, and greater hydrophobicity and diversity in the TRA chain
956 compared to $CD8^{+}CD5^{lo}$ cells. (**B-E**) Comparison of the TRAV gene segment usage (**B**), TRAJ
957 gene segment usage (**C**), TRBV gene segment usage (**D**), and TRBJ gene segment usage (**E**) within
958 TRA variable and TRB variable genes between $CD5^{hi}CD8^{+}$ (red) and $CD5^{lo}CD8^{+}$ (blue) cells. (**F-**
959 **J**) Comparison of CDR3α (left) or CDR3β (right) length in amino acids (**F**), CDR3 clonal overlap
960 by overlapped count matrix (**G**), top 20 CDR3 motifs (**H**), average hydrophobicity score (**I**) and
961 diversity (**J**) of CDR3α (left) and CDR3β (right) between $CD5^{hi}CD8^{+}$ and $CD5^{lo}CD8^{+}$ T cells. In
962 (**G**), number in cell indicates count number shared within the comparison group. (**H**) Occurrence
963 frequencies of the top 20 CDR3 motifs from mapped-CDR3α (left) and CDR3β (right) sequencings
964 in $CD5^{hi}CD8^{+}$ and $CD5^{lo}CD8^{+}$ cells, with the high-occurrence rate of the CDR3α motif
965 "SGGSNYKLTF" (underlined in red) specific to T1D-related IGRP peptide in the $CD8^{+}CD5^{hi}$
966 population. (**I**) Average hydrophobicity score defined by summing up the hydrophobicity score in
967 each amino acid in the CDR3 motif and dividing by the CDR3 length, then averaging by total
968 counts in each group. Diversity definition in (**J**) is shown in Materials and Methods section
969 Clonotype repertoire metrics formulas. In (**B-E**), each point represents 10 mice, with two points
970 for each group, totaling n = 20 mice (**F-J**) for all $CD5^{hi}$ or $CD5^{lo}$ samples. *$P < 0.05$, **$P < 0.01$,
971 ***$P < 0.001$, by two-way ANOVA (**B-E**), by Welch two sample t-test (**F**), and unpaired, two-

972 tailed t test (**I**) and (**J**).

973 **Figure 8 Thymocyte self-reactivity impacts the effector functions and memory cell formation**

974 **of auto-reactive T cells in the T1D model NOD mice.**

975

976 ## Table

977 **Table 1 Naïve $CD5^{hi}CD8^{+}$ and $CD5^{lo}CD8^{+}$ T cells exhibit distinct expression in**

978 **effector/memory T cell gene-expression clusters.**

Cluster	Characteristics	$CD5^{lo}$	$CD5^{hi}$	*P*	Proportion
I	Initial cytokine or effector response	2	21	6.66555E-45	0.913
II	Preparation for cell division	98	406	1.7815E-173	0.806
III	Cell cycle & division	81	175	2.20063E-29	0.684
IV	Naive and late memory	44	25	5.78321E-06	0.362
V	Early effector, late memory	33	150	2.31501E-70	0.820
VI	Short-term effector and memory	18	30	0.000881688	0.625
VII	Memory precursor	47	41	0.251118001	0.466
VIII	Naive or late effector or memory	103	98	0.492702408	0.488
IX	Short-term effector or memory	27	45	6.4806E-05	0.625
X	Late effector or memory	28	49	1.77113E-06	0.636

979

980 Variation in gene-expression clusters between naïve $CD5^{hi}CD8^{+}$ and $CD5^{lo}CD8^{+}$ T cells and gene-

981 set clusters in $CD8^{+}$ T cells evaluated by the Immunological Genome Project (published clusters

982 with designated characteristics). In the '$CD5^{lo}$' and '$CD5^{hi}$' columns, values represent the count of

983 genes predominantly expressed in each subset; 'Proportion' indicates the fraction of those genes

984 expressed in the $CD5^{hi}$ subset. Statistical significance of expression differences was determined

985 using the $\chi 2$ test (*P*).